Application of the Preisach Model to Ferroelectric Composites

Tsang Chun Ho

M. PHIL.

THE HONG KONG POLYTECHNIC UNIVERSITY

2003

Acknowledgments

It is my pleasure to express my grateful appreciation to Prof. F. G. Shin, my chief supervisor, who provides direction and guidance for my project.

I also wish to thank Mr. C. K. Wong and Mr. Y. T. Or for their valuable advice and encouragement to me.

This project is supported by a research grant of The Hong Kong Polytechnic University.

Contents

Abstract

The Preisach model [Preisach, 1935] has been successfully employed to study magnetic materials in which the phenomenon of hysteresis needs to be taken into account. Ferroelectric materials, the electric analog of magnetic materials, likewise exhibit hysteresis and field history dependence. The Preisach model is a mathematical model which provides a means for determining the highly nonlinear relationship between polarization and applied field. In this study, the Preisach model was used as a tool for modeling nonlinear behavior in ferroelectrics and ferroelectric composites.

In addition, a model of ferroelectric behavior based on a combination of the Preisach model and the Landau theory for the second order phase transition was developed so as to allow discussion on the effect of temperature on physical properties, which the Preisach model could not tackle. The Preisach model considers a material to be a collection of hysteretic units with square hysteresis loops having two polarization states (called Preisach hysterons). A Preisach hysteron is only endowed with electrical properties so that it cannot take into account other effects, such as temperature. On the other hand, the Landau theory [Lines and Glass, 1977] for ferroelectrics has been successful in explaining the thermodynamic properties of ferroelectrics near phase

transition temperatures, but it cannot describe minor loops. In this study, a new approach which combines the two models was suggested. In essence, Preisach hysterons were modified to become hysterons whose characteristics were described by the Landau theory, i.e. square-looped hysterons were replaced by hysteresis loops of the Landau theory. Thus, broad features of the Landau theory were included in the new model. This hybrid, Preisach-Landau model, allows discussion on phase transition, major and minor loops, and the effect of temperature on physical properties. Using this model, the *D-E* major and minor loops at different temperatures can be simulated. Also, the coercive field, remanent polarization and permittivity as a function of temperature may be calculated. In this model, the deletion property and the property of equal vertical chords of the classical Preisach model hold, but not the congruency property [Mayergoyz, 1991], the latter is nevertheless not so commonly observed in many real materials.

Some ferroelectric materials, such as triglycine sulfate (TGS), has a finite dielectric constant at the ferroelectric-paraelectric phase transition temperature T_c, which is in contra-distinction to the expectation of the Landau theory of (second order) phase transition. A more refined Preisach-Landau model was proposed to tackle features such as finite dielectric constant at T_c. Comparing with experimental results on TGS [Gaffar *et al.*, 1989], this modification produced a finite reciprocal dielectric constant at phase transition temperature as observed in experiments but the earlier Preisach-Landau model

could not. Also, this modification was able to account for finer features of the experimental $1/\varepsilon_r$-T curve while the general feature of the remanent polarization versus temperature curve was not affected.

We used the Preisach model to study the nonlinear dielectricity of the ferroelectric polymer polyvinylidene fluoride (PVDF) as an example. The electric displacement D in the material when subjected to a sinusoidal electric field of a given frequency was calculated. Both the in-phase and out-of-phase components as well as higher harmonics emerged naturally from the model calculation. D-E loops at different field amplitudes were simulated and Fourier analyzed. The Fourier coefficients obtained were compared with the experimental data of Furukawa *et al.* [Furukawa *et al.*, 1987]. Almost all the broad experimental features were reproduced by the simulations. A Preisach-Landau model was also used in this work, and the simulated results were compared with the results obtained from the Preisach model. Both simulations gave similar answers. It is remarkable that the power of the Preisach model was preserved in a Preisach-Landau model.

In the study of ferroelectric composites, first a multi-layered ferroelectric composite was studied by using the concepts of the Preisach model to describe each constituent material. Under the assumption that the free charge on each interface was constant, the theory for multi-layered ferroelectric composites was analyzed. The results obtained

were compared to *D-E* measurements made in the poling of polyvinylidenefluoride-trifluoroethylene (P(VDF-TrFE)) copolymer film sandwiched between ferroelectric triglycine sulfate crystal (TGS) electrodes [Ploss and Ploss, 1996]. In general, the computer simulations were in good agreement with experimental results. The *D-E* histories of the copolymer and the electrode material during poling were also obtained.

A Preisach-Landau model was also applied to tackle the 0-3 composite problem. We considered a composite comprising spherical ferroelectric inclusions in a linear dielectric matrix. A D.C. electric field E_p was applied to polarize a virgin TGS/polymer composite. Under this poling process, we considered different conditions to discuss the variation of physical behavior of the composite and its constituents. These included the effect of the poling field E_p, poling temperature T_p and conductivity σ_m of the matrix. We showed that the remanent polarization of the composite could be enhanced by increasing E_p, T_p and σ_m.

Chapter 1

Introduction

1.1 Background

Dielectric materials exhibiting hysteresis effect are known as ferroelectric materials, because their polarization versus electric field curves are so much like the magnetization versus magnetic field curves of ferromagnetic materials. All ferroelectric materials possess piezoelectricity, in which the polarization may be changed when it is mechanically strained, and pyroelectricity, in which the polarization may be changed when it is thermally strained.

In most virgin ferroelectric materials, the piezoelectric and pyroelectric effects are not appreciable so that they cannot be directly used in many applications. One common method for solving this is to polarize the materials as highly as possible to magnify the effects. In many applications, such as precision machining, the ferroelectrics are required to operate under high stress and high electric field. However, pronounced nonlinear dielectric properties and hysteresis behavior are evident in these conditions. For many materials, another problem is caused by the fact that the coercive field strength is only slightly lower than the electrical breakdown field strength. In addition, most ferroelectric

ceramic materials are brittle and possess cracks, and many exhibit brittle fracture. Many applications desire materials properties, which often are not obtained in single materials. Therefore, different materials are proposed to be combined to form a composite, taking the advantage of the favorable properties and limiting the detrimental properties of constituent materials. Thus the question of how to accurately predict the behavior of composites (in our case, ferroelectric composites) becomes important.

In the literature, a traditional approach is to analyze the properties of a ferroelectric composite based on the assumption that the nonlinear behavior of the constituents is not apparent, in other words, the electric fields in the constituents are small. For higher fields, the nonlinear dielectric properties and hysteresis behavior of ferroelectrics are evident. One approach is to write the electric displacement or polarization of a ferroelectric as a Taylor series of electric field. To discuss the properties of ferroelectrics under arbitrary fields, hysteresis models are needed.

Hysteresis effect has been observed in many different areas of science, e.g. ferromagnets, ferroelectrics, plastic materials, economics, chemistry and others. Hysteresis is a "history" dependent effect. "History" dependent effect implies that the output of a system cannot be expressed in terms of a single-valued function of the input to the system and is influenced by the history of the input. As illustrated in Figure 1.1(a), when the input of the system increases from zero, the output increases along the path $\mathcal{A}$.

The path $\mathcal{A}$ is called the virgin curve. When the input of the system reaches u_1, the system becomes (positively) saturated. When the input is gradually reduced from u_1, the output decreases but along a path different from the one followed during the increase. As the input is reduced to u_2, the system becomes (negatively) saturated. Thus, a new curve, path C, is traced out. If this cycle of operation is repeated, the curve eventually closes upon itself, i.e. if the input is then increased again to u_1, the system returns to positive saturation, and so on. The closed curve is called the major (or saturated) hysteresis loop. The size of this hysteresis loop is unchanged if the range of the input becomes larger. The paths $\mathcal{B}$ and C are called the major ascending curve and major descending curve respectively. In general, all hysteresis loops traceable by the system, such as the closed curve formed by the paths $\mathcal{D}$ and $\mathcal{E}$, must lie inside the major hysteresis loop of the system and are called minor hysteresis loops. Paths such as $\mathcal{D}$ and $\mathcal{E}$ are called reversal curves.

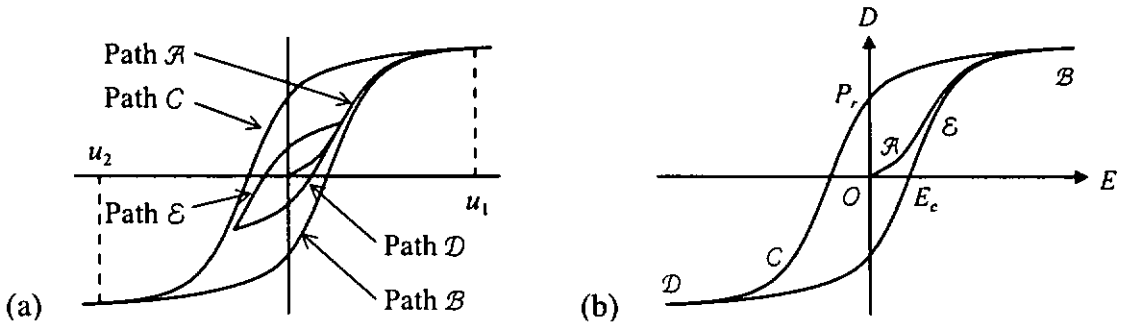

FIG. 1.1 (a) General character of hysteresis loop. (b) A ferroelectric D-E hysteresis loop.

In ferroelectric materials, hysteresis effect occurs in the relation between the applied electric field E and the electric displacement D (or polarization P), as shown in Figure 1.1(b). From Figure 1.1(b), when a field E is applied to polarize a virgin ferroelectric, the corresponding displacement D changes along the segment $\mathcal{OB}$. If E is small enough, the relation between E and D is reversible because the field E is not large enough to switch any ferroelectric domains in the material. The material behaves as a linear dielectric material, i.e. the D-E relation is linear (i.e. segment $\mathcal{OA}$). When the field E further increases, the D-E relation becomes nonlinear (i.e. segment $\mathcal{AB}$), and the rate of change of D in this segment is larger than that in the segment $\mathcal{OA}$. At the same time, domains in the material grow until all domains are combined to form a single domain. Thus, the material becomes positively saturated (i.e. point $\mathcal{B}$). As the field E is gradually reduced from the point $\mathcal{B}$, the single domain decomposes, and the displacement D is reduced simultaneously but along the segment $\mathcal{BCD}$. This is because the motion of domains is irreversible. At zero field, the displacement D has a non-zero value P_r, called the remanent polarization. Since a greater portion of domains is still aligned in the positive direction, the remanent polarization is positive. The field at which the displacement D is reduced to zero is $-E_c$. E_c is called the coercive field. Below this point, the corresponding D of the material changes sign (from positive to negative). At point $\mathcal{D}$, the material is polarized to negative saturation. Here, all domains are combined again as

in the case of positive saturation, but the sign of D is negative. If the field E increases again, the profile of D is the segment $\mathcal{DEB}$. The closed segment $\mathcal{BCDEB}$ forms a major (or saturated) D-E hysteresis loop of the material.

Hysteresis effect in ferroelectric materials is only exhibited below a certain temperature T_{tr}. When the temperature of the material is above T_{tr}, the remanent polarization of the material disappears and the material becomes paraelectric. If a ferroelectric material exhibits a hysteresis behavior (i.e. below T_{tr}), the material is in the ferroelectric phase. The phase transition between the ferroelectric phase and paraelectric phase is called a ferroelectric-paraelectric phase transition.

1.2 Scope and outline of this thesis

The present work involves the theoretical study of the hysteresis behavior in ferroelectrics and ferroelectric composites by using the concepts of the Preisach model. This chapter serves to introduce the modeling of hysteresis and the ideas behind several useful models.

In Chapter 2, a model of ferroelectric behavior based on a combination of the Preisach model and the Landau theory is developed so as to allow discussion on the effect of temperature on physical properties, which the Preisach model alone cannot tackle. We prefer to call this kind of a hybrid model a Preisach-Landau model, which, as

will become clear in later chapters, can have many variants.

In our study, the nonlinear dielectricity of the electric displacement of a ferroelectric is simulated by using the moving Preisach model and a Preisach-Landau model, as shown in Chapter 3. The results simulated are compared with the experimental data given by Furukawa *et al.* [Furukawa *et al.*, 1987]. This is indicative of the usefulness of the Preisach model and the Preisach-Landau model in studying ferroelectric (nonlinear) behavior.

Based on the foregoing experience with Preisach models, we analyze the *D-E* response of ferroelectric composites by using Preisach models (or Preisach-Landau models) to describe each constituent ferroelectric material. The study of ferroelectric composites is discussed in Chapter 4. The Preisach model is applied to study the *D-E* measurements made in the poling of a multi-layered composite and the simulations are compared with experimental results [Ploss and Ploss, 1996]. In addition, a Preisach-Landau model is used to study the poling of ferroelectric 0-3 composites. Under different conditions of poling, the electric displacements in the composite and in the constituent materials are studied with regard to the effect of the matrix conductivity, the poling field and the poling temperature. These processes in poling can be understood more succinctly in the light of the new model. This study seeks to establish a pioneering investigation of the hysteresis and other history dependent behaviors of ferroelectric composites.

1.3 Literature Review of Hysteresis Modeling

This section outlines some past research works on hysteresis modeling. We will introduce several popular mathematical hysteresis models, including the Preisach model, the Stoner-Wohlfarth (S-W) model and the Miller model. Moreover, we will introduce the Landau theory for phase transition of ferroelectrics.

1.3.1 Preisach model

Ferromagnetic hysteresis has long been studied. In 1887, Lord Rayleigh first proposed a model of ferromagnetic hysteresis. Another model was developed by Duhem at the turn of the century. One of the most successful mathematical models is the Preisach model first proposed by Preisach [Preisach, 1935] in 1935. It is able to describe major and minor loops. This model is limited by its deletion property and congruency property. However, many magnetic materials generally do not follow these properties exactly. For this reason, many modifications of the Preisach model have been suggested. The moving model [Mayergoyz, 1991; Bertotti, 1998] and the product model [Mayergoyz, 1991; Bertotti, 1998; Kadar, 2000] can remove the congruency property. Accommodation [Bertotti, 1998; Della Torre, 1994] and aftereffect [Bertotti, 1998] remove the deletion property. In addition, the complete moving Preisach model [Bertotti, 1998] is developed

to obtain more accurate hysteretic behavior.

In ferroelectric hysteresis studies, the earliest work making use of the Preisach model seems to be due to Turik [Turik, 1963, 1964a, 1964b]. For example, Turik in 1963 [Turik, 1963] applied the Preisach model to ferroelectrics under weak field. The Preisach function was expressed in a Maclaurin series, and the branches of minor loops and the dielectric loss were written in analytical expressions. A handful of papers seeking new applications of the Preisach model were published more recently. For instance, Huo [Huo, 1989] combined the Preisach model with the Landau theory of the first order phase transition to simulate the stress-strain curve and the strain-temperature curve of shape memory alloys. Freeman and Joshi [Freeman and Joshi, 1996] simulated the PZT electromechanical behavior based on the extended Preisach model in which the Preisach hysteron was modified in order to allow its polarization to vary with stress. Hughes and Wen [Hughes and Wen, 1997] applied the Preisach model to research hysteretic behavior of piezoceramics and shape memory alloys. Bartic *et al.* [Bartic *et al.*, 2001] developed a model based on a ferroelectric interpretation of the Preisach model and proposed an experimental method to determine the Preisach function.

As mentioned earlier, the Preisach model was proposed in 1935 [Preisach, 1935]. In the 1970s and 1980s, the mathematical properties of the Preisach model were examined and developed by the Russian mathematician Krasnoselskii [Krasnoselskii and

Pokrovskii, 1989]. The Preisach model, transcribed for use in ferroelectrics, considers a material to be a collection of square-loop hysterons having two normalized spontaneous polarization states: $\rho = -1$ and $\rho = +1$, as shown in Figure 1.2(a). Each hysteron is switched up if the external field E is increased to a value greater than the switch-up field U of the hysteron, and is switched down if the field is decreased to smaller than the switch-down field V of the hysteron.

An isolated hysteron has a well-defined coercive field, i.e. its P-E loop is symmetrically placed about $E = 0$ (thus $U = -V$). Since hysterons would be subjected to interaction fields due to other hysterons inside the material, individual P-E hysteresis loops are shifted along the E-axis. As a result, the magnitudes of the switching fields U and V may not be equal. Mathematically, U and V of each hysteron can be expressed as

$$U = E_{crit} + E_{int} \qquad \text{and} \qquad V = -E_{crit} + E_{int} \tag{1.1}$$

where E_{crit} is the critical (or coercive) field of the hysteron when isolated and E_{int} is the interaction field acting on the hysteron due to others. Thus E_{crit} and E_{int} are alternative coordinates for labeling a Preisach hysteron with switching fields U and V.

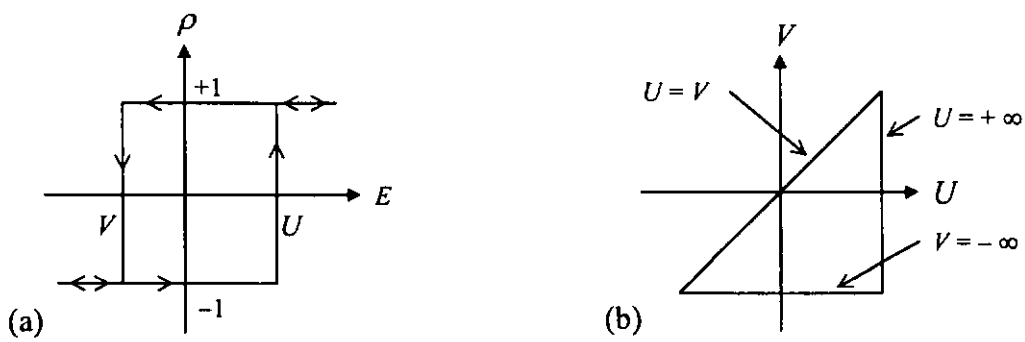

FIG. 1.2 (a) A single Preisach hysteron. (b) Preisach plane.

For an aggregation of hysterons, both E_{crit} and E_{int} of individual hysterons may be distributed, the latter depend on their environment, leading to a distribution of U and V. This distribution represents therefore the distribution of hysterons, which characterizes a ferroelectric material, and is described by the Preisach function $\mathcal{P}(U,V)$. This function is defined over the Preisach plane, which is the U-V plane with $U \geq V$, as shown in Figure 1.2(b). With this definition, all hysterons are switched up if a sufficiently large field E is applied to the material. Hence, the saturation polarization P_s equals the sum of the "switch-up" state of hysterons and is given by

$$P_s = \iint_{U \geq V} \rho(U,V,E)\, \mathcal{P}(U,V) dU dV = \int_{-\infty}^{\infty} \int_{-\infty}^{U} \mathcal{P}(U,V) dV dU . \tag{1.2}$$

The polarization of a ferroelectric material generally is the sum of the integral of $\mathcal{P}(U,V)$ weighted by $\rho = +1$ and $\rho = -1$ depending on the field history. To explain the polarization change in the hysterons, constructions on the Preisach plane is found to be convenient. A poling process in Figure 1.3(a) is shown as an example. First, a material is poled by an applied field β_1 such that its polarization becomes negative saturation. Then, a sequence of field is applied to the material and the corresponding P-E curve is shown in Figure 1.3(b). Figure 1.4 shows the behavior on the Preisach plane in each step of the process. The field E is initially decreased to β_1 (in the Figure 1.4(a) β_1 may be imagined to be $-\infty$), switching all hysterons down. As E increases to α_1 (Figure 1.4(b)), a vertical

line (conveniently representing an increasing field) sweeps along the U-axis changing the hysteron ρ's to +1. E is then decreased to β_2 (Figure 1.4(c)), a horizontal line (representing a decreasing field) sweeps down the V-axis changing the ρ's to -1. When E is increased to α_1 again (see Figure 1.4(d)), the ρ's change to +1 again. It follows that the Preisach plane is divided into two parts S^+ where each hysteron has $\rho = +1$, and S^- where each hysteron has $\rho = -1$. Mathematically, the polarization is given by

$$P(E) = \iint_{S^+} \rho(U,V,E)\, \mathcal{P}(U,V)dUdV$$

$$= \iint_{S^+} \mathcal{P}(U,V)dUdV - \iint_{S^-} \mathcal{P}(U,V)dUdV \qquad (1.3)$$

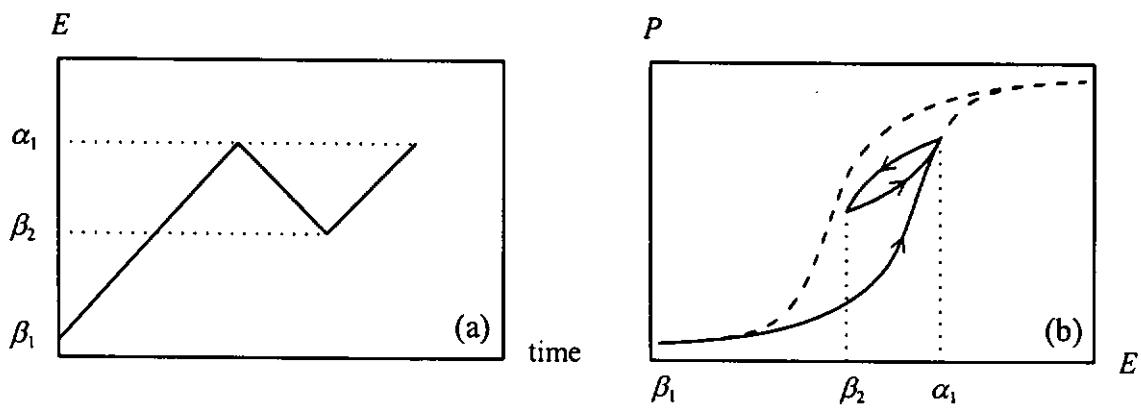

FIG. 1.3 (a) A field history is applied to a material in a poling process. (b) The solid line denotes the P-E history during the poling process. The dashed line denotes the major loop of the material.

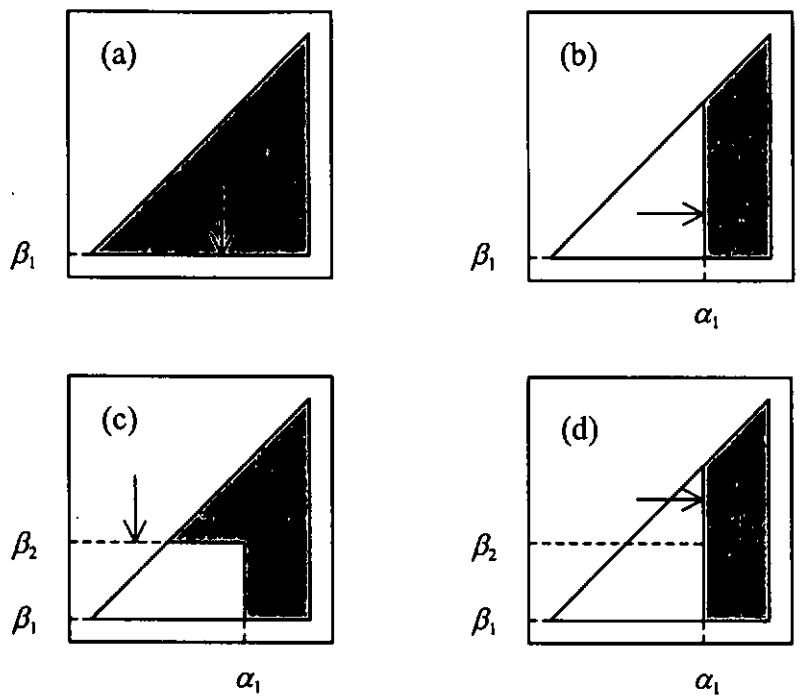

FIG. 1.4 The corresponding status of the Preisach plane after applying (a) β_1, (b) α_1, (c) β_2 and (d) α_1. The gray and white regions in the *U-V* plane (or E_{crit}-E_{int} plane) denote regions in which $\rho = -1$ and $\rho = +1$ respectively.

The Preisach model is characterized by the deletion property and congruency property. It has been shown that the necessary and sufficient condition for the validity of this model is that the deletion property and congruency property hold [Mayergoyz, 1991]. The deletion property [Mayergoyz, 1991] is that the output of a model is only affected by the alternating series of dominant input extrema. The effects of all other inputs are wiped out. As illustrated in Figure 1.4(d), when E increases from β_2 to α_1, the distribution of S^+ and S^- in the Preisach plane is the same as the distribution at α_1, thus the two outputs of the model are the same. In other words, the final output of the model is the output at α_1 after the whole field history is applied, and the field β_2 does not affect the final

output of the model, i.e. β_2 is wiped out. The congruency property [Mayergoyz, 1991] is that all minor loops between the same pair of external fields are congruent.

Since the hysteretic behavior of ferroelectrics is defined by the Preisach function, a very important question associated with the modeling is the "identification" problem. The aim is to find the "shape" of the Preisach function. The identification strategies are divided into two classes: (i) parametric identification and (ii) interpolation identification.

(i) Parametric identifications [Oti *et al.*, 1991; Della Torre and Vajda, 1994; Della Torre, 1999;] use knowledge about physical processes to determine the Preisach functions, which characterize the process, and use experimental data to find the parameters of these functions. Common distribution functions can be found in the literature [Basso and Bertotti, 1994; Cornejo *et al.*, 1997; Andrei and Stancu, 2000].

(ii) Interpolation identifications [Bate, 1962; Chen and Lynch, 1998; Della Torre, 1999] interpolate experimental data. In the Preisach model, this kind of identifications is very difficult to use because the Preisach function is the second partial derivative of the polarization (see Equation (1.3)). For example, one method [Della Torre, 1999] requires taking the second partial derivative of the polarization resulting from first-order reversal curves. This method is very sensitive to experimental error.

1.3.2 Stoner-Wohlfarth model

The Stoner-Wohlfarth (S-W) model [Bertotti, 1998; Della Torre, 1999; Mayergoyz, 1991] is also quite successful in ferromagnetic hysteresis modeling. In the S-W model, a magnetic material is considered as a collection of single-domain uniaxial magnetic particles, called S-W particles. Since a S-W particle is amenable to a formal physical description, the S-W model is popular in magnetic hysteresis research and is usually regarded as a physical model.

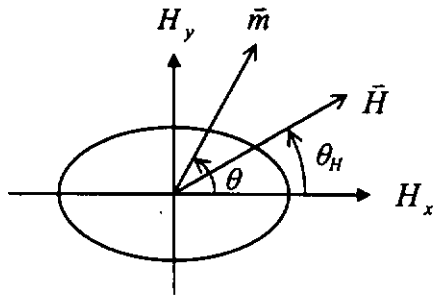

FIG. 1.5 A single S-W particle

In the S-W model, the S-W particle is an ellipsoid (see Figure 1.5). Its long axis is assumed to align with the easy magnetization direction. When the applied magnetic field $\vec{H}$ changes, the magnetization $\vec{m}$ of the particle changes. Note that $\vec{m}$ is aligned with the easy axis under zero field. Since a S-W particle is assumed to be single domain, the magnitude of $\vec{m}$ is constant, say m_s. The free energy G of the particle is divided into two parts: anisotropy energy $K\sin^2\theta$ and the energy of interaction between $\vec{H}$ and $\vec{m}$, i.e.

$$G = K\sin^2\theta - \vec{m}\cdot\vec{H} \tag{1.4}$$

where θ is the angle between the easy axis and $\vec{m}$, and $K > 0$ is the anisotropy constant.

The equilibrium magnetization corresponds to minimum free energy G, i.e.

$$\frac{\partial G}{\partial \theta} = 2K \sin\theta \cos\theta + m_s H_x \sin\theta - m_s H_y \cos\theta = 0 \tag{1.5}$$

where H_x and H_y are the x- and y-components of $\vec{H}$. H_x is parallel to the easy axis. Let $\alpha = \frac{2K}{m_s}$. Then, Equation (1.5) becomes

$$-\frac{H_x}{\cos\theta} + \frac{H_y}{\sin\theta} = \alpha . \tag{1.6}$$

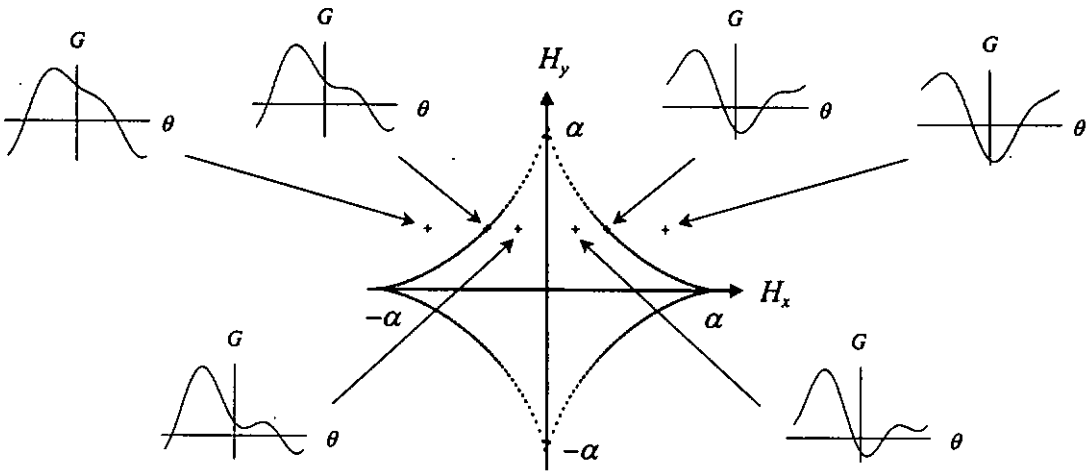

FIG. 1.6 The G-θ graphs on the side give the profile of the free energy $G(\theta)$ (see Equation 1.4) at point (H_x, H_y) in the H_x-H_y plane. The dotted line denotes the astroid curve described by Equation (1.8).

From Figure 1.6, we see that, in the interior of some region (bounded by an astroid curve), G has two or more minima. G has only one minimum outside the region. So, the condition for only one minimum of G is $\partial^2 G / \partial^2 \theta = 0$. Thus, by differentiating Equation (1.6) with respect to θ, we have

$$\frac{H_x}{\cos^3\theta} + \frac{H_y}{\sin^3\theta} = 0 . \tag{1.7}$$

Solving Equations (1.6) and (1.7), we get

$$H_x^{2/3} + H_y^{2/3} = \alpha^{2/3} \tag{1.8}$$

which is the equation of the astroid curve. Using this curve, the magnetization m_H of the particle along the applied field direction can be calculated for any given θ_H (Figure 1.7).

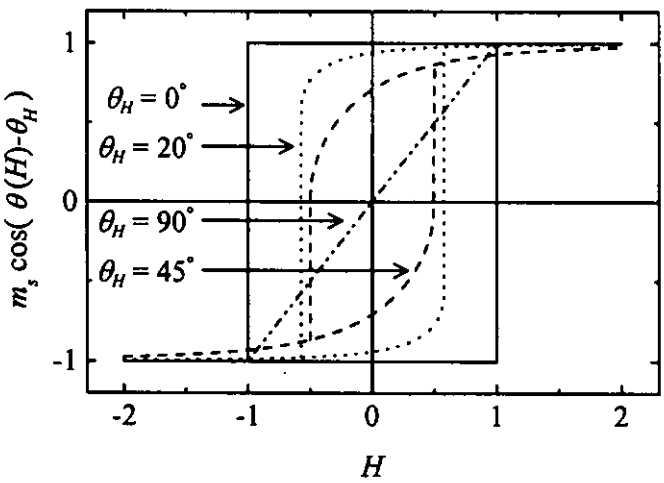

FIG. 1.7 The magnitude of the magnetization of S-W particle, $m_H = m_s \cos(\theta(\bar{H}) - \theta_H)$, at different θ_H (Here m_s and α are assumed to be 1).

The S-W model considers an infinite set of the S-W particles in a material. Since the hysteresis loop of the S-W particle depends on α and θ, the distribution of S-W particles is thus defined by a function $\xi(\alpha,\theta)$. Therefore, the magnetization $\bar{M}$ of a S-W material is given by

$$\bar{M}(\bar{H}) = \iint \bar{m}_H(\alpha,\theta,\bar{H})\xi(\alpha,\theta)\, d\alpha d\theta \tag{1.9}$$

where $\bar{m}_H$ is the magnetization of a S-W particle parallel to $\bar{H}$. As the S-W model do not consider the interaction among the particles, the model can describe symmetric loops, but not asymmetric loops. A modification of the model is to incorporate an interaction

field $\bar{H}_i$ to the S-W particle. Thus, the magnetization $\bar{M}$ of a S-W material becomes

$$\bar{M}(\bar{H}) = \iiint \bar{m}_H(\alpha,\theta,\bar{H}_i,\bar{H})\xi(\alpha,\theta)\, d\alpha d\theta d\bar{H}_i \,. \tag{1.10}$$

1.3.3 Miller model

The Miller model was proposed by Miller *et al.* [Miller *et al.*, 1990, 1991] a decade ago. In the Miller model, the electric displacement D of a ferroelectric is written as

$$D(E) = \varepsilon_0 \varepsilon_f E + P_d(E) \tag{1.11}$$

where E is an applied electric field, and P_d is the polarization due to switching dipoles only. $\varepsilon_f = 1 + \chi_f$ is the linear dielectric constant of the ferroelectric, where χ_f is the susceptibility. The polarization P_d at the field E must lie on or within the major (or saturated) hysteresis loop, whose branches (i.e. ascending major curve and descending major curve) are assumed to be anti-symmetric. The latter relationship between the ascending major curve P_{sat}^+ and descending major curve P_{sat}^- may be written as

$$P_{sat}^+(E) = -P_{sat}^-(-E) \tag{1.12}$$

In the absence of a physical theory for predicting dipole switching properties as a function of E, a convenient expression for $P_{sat}^+(E)$ which can approximate a major branch is

$$P_{sat}^+(E) = P_s \tanh\left[\frac{E - E_c}{2\delta}\right] \tag{1.13}$$

where $\delta = E_c\left[\ln\left(\frac{1+P_r/P_s}{1-P_r/P_s}\right)\right]^{-1}$, and E_c, P_r and P_s are the coercive field, remanent

polarization and saturation polarization of the material respectively. In the Miller model, the derivative of P_d with respect to E on a polarization curve is confined to a value between those of the major ascending and descending curves at the same E. In other words, all polarization curves are modeled by some scaling of the major ascending (or descending) polarization curve. Thus, mathematically, the derivative of P_d is given by

$$\frac{\partial P_d(E)}{\partial E} = \Gamma \frac{\partial P_{sat}(E)}{\partial E} \tag{1.14}$$

where $P_{sat}(E)$ is the polarization on the major hysteresis loop at the applied field E; here $P_{sat}(E) = P_{sat}^{+}(E)$ for an increasing field and $P_{sat}(E) = P_{sat}^{-}(E)$ for a decreasing field. Γ is a scaling function with value between 0 and 1, and is taken as

$$\Gamma = 1 - \tanh\left[\left(\frac{P_d - P_{sat}}{\xi P_s - P_d}\right)^{1/2}\right] \tag{1.15}$$

where $\xi = +1$ for an increasing field and $\xi = -1$ for a decreasing field.

1.3.4 Landau theory for phase transition

In the Landau theory, the fundamental assumption is that, in the vicinity of the critical (transition) point, the free energy G of a ferroelectric material is an analytic function of the electric displacement D of the material. Therefore, we can express G as the Taylor series of D, i.e.

$$G = G_0 + \frac{1}{2}\alpha D^2 + \frac{1}{4}\beta D^4 + \frac{1}{6}\gamma D^6 + \cdots. \tag{1.16}$$

Here α is frequently expressed as a function of temperature T in the form of

$\alpha = \alpha_0(T - T_c)$ where $\alpha_0 > 0$ and T_c is the Curie temperature. In a ferroelectric, the transition can be first or second order. The order of the transition is determined by the sign of β. We start the discussion by considering second order transition. Here β is positive, and the free energy G is

$$G = G_0 + \frac{1}{2}\alpha D^2 + \frac{1}{4}\beta D^4 \tag{1.17}$$

where the sixth and higher order terms are ignored. The conditions for a minimum G are $\partial G/\partial D = 0$ and $\partial^2 G/\partial D^2 > 0$ which imply

$$D = \pm\sqrt{-\alpha/\beta} = \pm\sqrt{\alpha_0(T_c - T)/\beta} \tag{1.18}$$

and $\partial^2 G/\partial D^2 = \alpha + 3\beta D^2 = \alpha_0(T - T_c) + 3\beta D^2 > 0$. (1.19)

In the ferroelectric phase ($T < T_c$), the remanent polarization of the material is $\sqrt{\alpha_0(T_c - T)/\beta}$ (from Equation (1.18)). The reciprocal permittivity ε^{-1} is calculated from $\partial^2 G/\partial D^2$. Using Equations (1.18) and (1.19), $\varepsilon^{-1} = 2\alpha_0(T_c - T)$. In the paraelectric phase ($T > T_c$), $\varepsilon^{-1} = \alpha_0(T - T_c)$. We see that the slope of the reciprocal permittivity curve in the ferroelectric phase is twice that in the paraelectric phase.

In the first order transition, the free energy G is written as

$$G = G_0 + \frac{1}{2}\alpha D^2 + \frac{1}{4}\beta D^4 + \frac{1}{6}\gamma D^6 \tag{1.20}$$

where β is negative and γ is positive. At the first order phase transition temperature T_{tr}, the free energy G in the ferroelectric phase and in the paraelectric phase are the same. From Equation (1.20), we have

$$\frac{1}{2}\alpha_0(T_{tr}-T_c)D_r^{\ 2}+\frac{1}{4}\beta D_r^{\ 4}+\frac{1}{6}\gamma D_r^{\ 6}=0 \tag{1.21}$$

where D_r is the remanent polarization at $T = T_{tr}$. Also, the condition for a minimum G is $\partial G/\partial D = 0$, i.e.

$$\alpha_0(T_{tr}-T_c)D_r+\beta D_r^{\ 3}+\gamma D_r^{\ 5}=0. \tag{1.22}$$

Solving Equations (1.21) and (1.22),

$$D_r^{\ 2}=-\frac{3\beta}{4\gamma}. \tag{1.23}$$

Substituting Equation (1.23) into (1.21), we have

$$T_{tr}=T_c+\frac{3\beta^2}{16\alpha_0\gamma}. \tag{1.24}$$

In the ferroelectric phase ($T < T_{tr}$), the remanent polarization of the material is $\sqrt{(-\beta+\sqrt{\beta^2-4\alpha\gamma})/2\gamma}$. It is clear that the remanent polarization at T_{tr} is $\sqrt{-3\beta/4\gamma}$.

The reciprocal permittivity ε^{-1} is

$$\varepsilon^{-1}=\left.\frac{\partial^2 G}{\partial D^2}\right|_{D=D_r}=8\alpha_0(T_{tr}-T)+\frac{3\beta^2}{4\gamma}. \tag{1.25}$$

In the paraelectric phase ($T > T_{tr}$), the reciprocal permittivity ε^{-1} is

$$\varepsilon^{-1}=\left.\frac{\partial^2 G}{\partial D^2}\right|_{D=0}=\alpha_0(T-T_{tr})+\frac{3\beta^2}{16\gamma}. \tag{1.26}$$

We see that, at $T = T_{tr}$, the reciprocal permittivity in the ferroelectric phase is four times that in the paraelectric phase. And, the slope of the reciprocal permittivity curve in the ferroelectric phase is eight times that in the paraelectric phase.

Chapter 2

A model of ferroelectric behavior based on a combination of the Preisach model and the Landau theory

2.1 Introduction

The Landau theory is a popular phenomenological theory for describing the thermodynamic properties of ferroelectrics near phase transition temperatures. It provides a basis for explaining the broad features of the thermodynamic properties, such as spontaneous polarization, coercive field and dielectric constant; but the predictions do not necessarily agree quantitatively with experimental observations. For example, in the study of coercive field, many experiments indicate that the experimental values are several orders of magnitude lower than the values calculated from the Landau theory [Jona and Shirane, 1962; Kim *et al.*, 2002]. In the study of triglycine sulfate (TGS), it is observed in many investigations that the dielectric constant ε_r has a finite value at the phase transition temperature T_c [Chincholkar and Unruh, 1968; Mansingh and Eswar Prasad, 1977]. Also, the ratio of the slope of the $1/\varepsilon_r$-T plot below T_c to that above T_c is not exactly two [Triebwasser, 1958; Gonzalo, 1970], in slight disagreement with the

Landau prediction for a second order ferroelectric material. Many more experimental observations show deviations from the Landau theory. On the other hand, the Preisach model [Preisach, 1935], quite widely used in studies of ferroelectric hysteresis research, provides a means for determining the highly nonlinear relationship between polarization and applied field in a ferroelectric material. In the Preisach model, a material is considered to be a collection of square-loops with two normalized polarization states, called hysterons. A "Preisach" hysteron is only endowed with electrical properties so that it can react to electrical excitations. It is not clear how a variation in temperature or mechanical stress can affect a system of hysterons.

In this chapter, we modify the "Preisach" hysterons to hysterons whose characteristics are described by the Landau theory of the second order phase transition for ferroelectrics. In this way, the effect of temperature on major and minor loops can be taken into account. Since "Landau" hysterons display the characteristics of ferroelectrics, a better connection with the physics of ferroelectrics is achieved. Using this model, the *D-E* major loops at different temperatures are calculated. Coercive field, remanent polarization and reciprocal dielectric constant are studied as a function of temperature, and are found to agree with the features calculated with the Landau theory. The deletion property, an elegant result of the classical Preisach model, can be proved in our model; however, the congruency property is not preserved. Also, our model preserves the

property of equal vertical chords of the nonlinear Preisach model. The following section introduces the ideas and formulation of a Preisach-Landau model.

2.2 Preisach-Landau model

2.2.1 "Landau" hysteron

To benefit from both theories (i.e. Preisach's and Landau's), we replace, in our model, Preisach hysterons by ones whose characteristics are described by the Landau theory, i.e. square-loops are to become Landau hysteresis loops. Thus, the broad features of both the Landau theory and the Preisach model are included in the new model. This hybrid, "Preisach-Landau" model, allows the discussion of field history dependence as well as temperature dependence of ferroelectric behavior.

In the Landau theory, the free energy G of a hysteron is written in terms of the electric displacement μ and temperature T as, for second order phase transition,

$$G(\mu,T) = G_0 - \frac{1}{2}\alpha\mu^2 + \frac{1}{4}\beta\mu^4, \tag{2.1}$$

where $\alpha = \alpha_0(T_c - T)$ and T_c is the Curie temperature and $\alpha_0, \beta > 0$. The applied field E is given by

$$E = \frac{\partial G}{\partial \mu} = -\alpha\mu + \beta\mu^3. \tag{2.2}$$

We call a hysteron whose hysteresis behavior is described by Equation (2.2) simply a "Landau" hysteron. Using Cardano's formula, the roots of Equation (2.2) are given by

$$\mu_j(\alpha,\beta,E) = \frac{2\mu_r}{\sqrt{3}}\cos\left[\frac{1}{3}\cos^{-1}\left(\frac{E}{E_{crit}}\right)+\delta\right], \qquad j = 1, 2, 3 \tag{2.3}$$

where $E_{crit} = 2\left(\frac{1}{3}\right)^{3/2}\frac{\alpha^{3/2}}{\sqrt{\beta}}$, $\mu_r = \sqrt{\frac{\alpha}{\beta}}$ and $\delta = \frac{2(j-1)\pi}{3}$.

When the temperature T is below the Curie temperature T_c, the electric displacement $\mu(E)$ is hysteretic. Otherwise, $\mu(E)$ is non-hysteretic. Every Landau hysteron has therefore two forms (see Figure 2.1).

(i) For $T < T_c$, it is clear that the critical field of the hysteron is E_{crit} and the remanent polarization is μ_r. Analyzing Equation (2.3), the electric displacement corresponding to the "switch-up" state is

$$\mu(E) = \frac{2\mu_r}{\sqrt{3}}\cos\left[\frac{1}{3}\cos^{-1}\left(\frac{E}{E_{crit}}\right)\right], \tag{2.4}$$

and for the "switch-down" state is

$$\mu(E) = \frac{2\mu_r}{\sqrt{3}}\cos\left[\frac{1}{3}\cos^{-1}\left(\frac{E}{E_{crit}}\right)+\frac{2\pi}{3}\right]. \tag{2.5}$$

(ii) For $T > T_c$, we note that $\mu(E)$ is non-hysteresis, so E_{crit} and μ_r do not have the meanings of critical field and remanent polarization respectively. They are complex numbers (pure imaginary). Analyzing Equation (2.3), the electric displacement is

$$\mu(E) = \frac{2\mu_r}{\sqrt{3}}\cos\left[\frac{1}{3}\cos^{-1}\left(\frac{E}{E_{crit}}\right)+\frac{4\pi}{3}\right]. \tag{2.6}$$

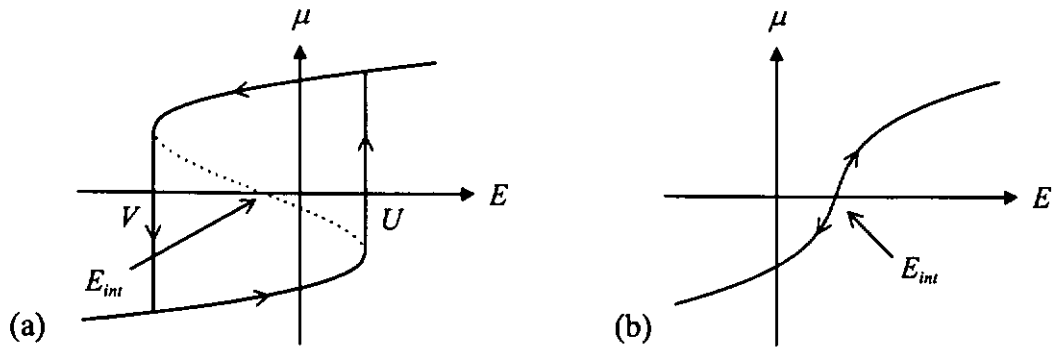

FIG. 2.1 A single "Landau" hysteron under an interaction field E_{int} at temperature (a) $T < T_c$, and (b) $T > T_c$. Note that $U = E_{crit} + E_{int}$ and $V = -E_{crit} + E_{int}$.

2.2.2 The electric displacement of a Preisach-Landau material at a fixed temperature

In the Preisach model, the Preisach function represents the distribution of hysterons, and its parameters are coercive field and interaction field. We follow this line of thinking to discuss parameters in the distribution of Landau hysterons and to formulate the calculation of electric displacement of a ferroelectric material described by a Preisach-Landau model.

The hysteresis loop of a Landau hysteron depends on α and β. Interactions among hysterons inside a material result in hysteresis loops that are shifted along the E-axis (see Figure 2.1) as in the Preisach model. The interaction is modeled as an interaction field E_{int}. Therefore, the net field applied on the hysteron should be $E - E_{int}$ when a field E is applied on the ferroelectric material. In other words, E is replaced by $E - E_{int}$ in Equation (2.2). As a result, the hysteresis loop of the Landau hysteron depends on α, β and E_{int}. The distribution of Landau hysterons is thus defined by a function $L(\alpha, \beta, E_{int})$

and its parameter space is three-dimensional. We assume the three variables are independent of each other, thus the distribution can be written as

$$\mathcal{L}(\alpha,\beta,E_{int}) = \mathcal{L}_{\alpha}(\alpha)\mathcal{L}_{\beta}(\beta)\mathcal{L}_{int}(E_{int}). \tag{2.7}$$

(i) For $T < T_c$, the electric displacement $D(E)$ of a Preisach-Landau material is given by

$$D(E) = \int_0^{\infty}\int_0^{\infty}\int_{-\infty}^{\infty} \mu(\alpha,\beta,E-E_{int})\,\mathcal{L}_{\alpha}(\alpha)\mathcal{L}_{\beta}(\beta)\mathcal{L}_{int}(E_{int})\,dE_{int}d\beta d\alpha. \tag{2.8}$$

In Equation (2.8), the expression of $D(E)$ contains three parameters, α, β and E_{int}. It is very inconvenient to determine the region S^+ where each hysteron is switched up and the region S^- where each hysteron is switched down. It is useful to transform from the α-β-E_{int} space to the E_{crit}-E_{int} plane (see Chapter 1). By the definitions of E_{crit} and μ_r, α and β are expressed in terms of E_{crit} and μ_r as

$$\alpha = \frac{3\sqrt{3}E_{crit}}{2\mu_r} > 0 \qquad \text{and} \qquad \beta = \frac{3\sqrt{3}E_{crit}}{2\mu_r^{\,3}} > 0. \tag{2.9}$$

It follows that

$$\mathcal{L}_{\alpha}(\alpha)\mathcal{L}_{\beta}(\beta)\,d\beta d\alpha = \frac{27E_{crit}}{2\mu_r^{\,5}}\mathcal{L}_{\alpha}\left(\frac{3\sqrt{3}E_{crit}}{2\mu_r}\right)\mathcal{L}_{\beta}\left(\frac{3\sqrt{3}E_{crit}}{2\mu_r^{\,3}}\right)d\mu_r dE_{crit}. \tag{2.10}$$

Let $\mathcal{L}_{\alpha\beta}(E_{crit},\mu_r) = \frac{27E_{crit}}{2\mu_r^{\,5}}\mathcal{L}_{\alpha}\left(\frac{3\sqrt{3}E_{crit}}{2\mu_r}\right)\mathcal{L}_{\beta}\left(\frac{3\sqrt{3}E_{crit}}{2\mu_r^{\,3}}\right)$. The range of each of the variables E_{crit} and μ_r is from 0 to ∞. Using Equations (2.3), (2.8) and (2.10), the electric displacement $D(E)$ becomes

$$D(E) = \int_0^\infty \int_{-\infty}^\infty \int_0^\infty \frac{2\mu_r}{\sqrt{3}} \cos\left[\frac{1}{3}\cos^{-1}\left(\frac{E - E_{int}}{E_{crit}}\right) + \delta\right]$$

$$\times \mathcal{L}_{\alpha\beta}(E_{crit}, \mu_r)\, \mathcal{L}_{int}(E_{int})\, d\mu_r dE_{int} dE_{crit}$$

$$= \int_0^\infty \int_{-\infty}^\infty \frac{2}{\sqrt{3}} \cos\left[\frac{1}{3}\cos^{-1}\left(\frac{E - E_{int}}{E_{crit}}\right) + \delta\right] \mathcal{L}_{crit}(E_{crit}) \mathcal{L}_{int}(E_{int})\, dE_{int} dE_{crit}$$

(2.11)

where $\mathcal{L}_{crit}(E_{crit}) = \int_0^\infty \mu_r\, \mathcal{L}_{\alpha\beta}(E_{crit}, \mu_r)\, d\mu_r$, and δ depends on the state of hysteron (see Equations (2.4)-(2.6)). The parameter space of $D(E)$ is now the E_{crit}-E_{int} plane.

(ii) For $T > T_c$, $\alpha = \alpha_0(T_c - T)$ is negative, and E_{crit} and μ_r are complex numbers (pure imaginary). Then, Equation (2.11) contains complex variables. Let $\tilde{\alpha} = -\alpha$, $\tilde{E}_{crit} = -iE_{crit}$ and $\tilde{\mu}_r = i\mu_r$, where $i = \sqrt{-1}$. Then $\tilde{\alpha}$, $\tilde{E}_{crit}$ and $\tilde{\mu}_r$ are positive real numbers. Using these variables, the expression of $D(E)$ does not contain complex variables. It becomes

$$D(E) = \int_0^\infty \int_0^\infty \int_{-\infty}^\infty \mu(-\tilde{\alpha}, \beta, E - E_{int})\, \mathcal{L}_\alpha(\tilde{\alpha}) \mathcal{L}_\beta(\beta) \mathcal{L}_{int}(E_{int})\, dE_{int} d\beta d\tilde{\alpha}\ . \quad (2.12)$$

By the definitions of $\tilde{E}_{crit}$ and $\tilde{\mu}_r$, $\tilde{\alpha}$ and β are

$$\tilde{\alpha} = \frac{3\sqrt{3}\tilde{E}_{crit}}{2\tilde{\mu}_r} > 0 \qquad \text{and} \qquad \beta = \frac{3\sqrt{3}\tilde{E}_{crit}}{2\tilde{\mu}_r^{\,3}} > 0\,. \qquad (2.13)$$

Now, $D(E)$ is given by

$$D(E) = \int_0^\infty \int_{-\infty}^\infty \frac{2i}{\sqrt{3}} \cos\left[\frac{1}{3}\cos^{-1}\left(i\frac{E - E_{int}}{\tilde{E}_{crit}}\right) + \frac{4\pi}{3}\right] \mathcal{L}_{crit}(\tilde{E}_{crit}) \mathcal{L}_{int}(E_{int})\, dE_{int} d\tilde{E}_{crit}$$

(2.14)

where $\mathcal{L}_{crit}(\widetilde{E}_{crit}) = \int_0^\infty \widetilde{\mu}_r \, \mathcal{L}_{\alpha\beta}(\widetilde{E}_{crit}, \widetilde{\mu}_r) \, d\widetilde{\mu}_r$. The parameter space of $D(E)$ is again the $\widetilde{E}_{crit}$-E_{int} plane.

2.2.3 Dielectric permittivity at a fixed temperature

The dielectric permittivity of a material is defined as the slope of $D(E)$, i.e. $\partial D/\partial E$. When the temperature T is below the Curie temperature T_c, the $D(E)$ curve of the material is hysteretic. Otherwise, it is non-hysteretic. The dielectric permittivity has therefore two forms.

(i) For $T < T_c$, the change in electric displacement in a Preisach-Landau material due to an increment in applied field is the sum of two contributions: one from "switching" hysterons and the other from "non-switching" hysterons. The reason is that the characteristics of Landau hysterons are different from Preisach hysterons. A Preisach hysteron is a bistable unit with μ equal to either $+1$ or -1. A Landau hysteron is also a bistable unit, but its μ in either the up or down state depends on applied field E (see Equations (2.4) and (2.5)). When a field increment is applied to the material, some hysterons are switched. The remainder do not change their states; however, their electric displacements change. This leads to the distinction between "switching" permittivity ε_s contributed from switched hysterons and "non-switching" permittivity ε_n from non-switched hysterons. The expression for the "non-switching" permittivity is

$$\varepsilon_n(E) = \int_0^{\infty}\int_{-\infty}^{\infty} \frac{\partial}{\partial E}\left\{\frac{2}{\sqrt{3}}\cos\left[\frac{1}{3}\cos^{-1}\left(\frac{E-E_{int}}{E_{crit}}\right)+\delta\right]\right\} \mathcal{L}_{crit}(E_{crit})\mathcal{L}_{int}(E_{int})\, dE_{int}dE_{crit}$$

$$= \iint_{S^+} \frac{\partial}{\partial E}\left\{\frac{2}{\sqrt{3}}\cos\left[\frac{1}{3}\cos^{-1}\left(\frac{E-E_{int}}{E_{crit}}\right)\right]\right\} \mathcal{L}_{crit}(E_{crit})\mathcal{L}_{int}(E_{int})dE_{int}dE_{crit} +$$

$$\iint_{S^-} \frac{\partial}{\partial E}\left\{\frac{2}{\sqrt{3}}\cos\left[\frac{1}{3}\cos^{-1}\left(\frac{E-E_{int}}{E_{crit}}\right)+\frac{2\pi}{3}\right]\right\} \mathcal{L}_{crit}(E_{crit})\mathcal{L}_{int}(E_{int})dE_{int}dE_{crit}$$

(2.15)

The expression for "switching" permittivity depends on the applied field history in the material. Assume that E_0 and E_1 are two successive extrema of the field history and $E_0 < E_1$. If the applied field E is an increasing field and $E_0 \le E < E_1$, then the "switching" permittivity of the material is

$$\varepsilon_s(E) = \frac{\sqrt{3}}{2}\int_{E_0}^{E} \mathcal{L}_{crit}\left(\frac{E-V}{2}\right)\mathcal{L}_{int}\left(\frac{E+V}{2}\right)dV. \tag{2.16}$$

Now, assume that E_1 and E_2 are two successive extrema of the field history and $E_1 > E_2$. If the applied field E is a decreasing field and $E_1 \ge E > E_2$, then the "switching" permittivity is

$$\varepsilon_s(E) = \frac{\sqrt{3}}{2}\int_{E}^{E_1} \mathcal{L}_{crit}\left(\frac{U-E}{2}\right)\mathcal{L}_{int}\left(\frac{U+E}{2}\right)dU. \tag{2.17}$$

Now, consider a virgin material on which a field E is applied. Since it starts from a state of zero polarization, we assume its initial state is well represented by the configuration shown in Figure 2.2(a) on the Preisach plane, in which half of the hysterons are "up" and half "down". Figures 2.2(b) and (c) show the corresponding status of the Preisach plane after applying E. If the applied field E is positive, then the

"switching" permittivity is (see Figure 2.2(b))

$$\varepsilon_s(E) = \frac{\sqrt{3}}{2}\int_{-E}^{E} \mathcal{L}_{crit}\left(\frac{E-V}{2}\right)\mathcal{L}_{int}\left(\frac{E+V}{2}\right)dV. \tag{2.18}$$

Otherwise, the "switching" permittivity is (see Figure 2.2(c))

$$\varepsilon_s(E) = \frac{\sqrt{3}}{2}\int_{E}^{-E} \mathcal{L}_{crit}\left(\frac{U-E}{2}\right)\mathcal{L}_{int}\left(\frac{U+E}{2}\right)dU. \tag{2.19}$$

(ii) For $T > T_c$, the μ-E relation of each hysteron is non-hysteretic. The permittivity of a hysteron only contains the "non-switching" part. The permittivity of the material is given by

$$\varepsilon(E) = \varepsilon_n(E) = \int_0^{\infty}\int_{-\infty}^{\infty}\frac{\partial}{\partial E}\left\{\frac{2i}{\sqrt{3}}\cos\left[\frac{1}{3}\cos^{-1}\left(i\frac{E-E_{int}}{\tilde{E}_{crit}}\right)+\frac{4\pi}{3}\right]\right\}$$

$$\times \mathcal{L}_{crit}(\tilde{E}_{crit})\mathcal{L}_{int}(E_{int})\, dE_{int}\, d\tilde{E}_{crit}. \tag{2.20}$$

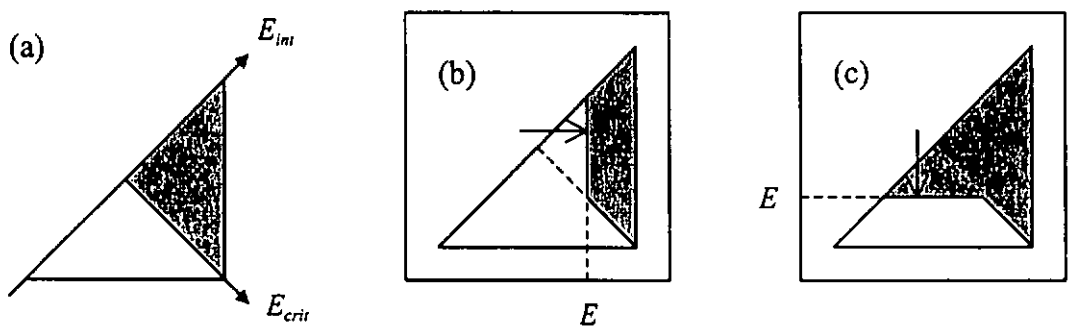

FIG. 2.2 (a) The status of the Preisach plane for a virgin material. The corresponding status of the Preisach plane for a virgin material after applying (b) an increasing field E and (c) a decreasing field E. The gray and white regions in the E_{crit}-E_{int} plane (or U-V plane) denote regions in which $\mu = -1$ and $\mu = +1$ respectively.

2.2.4 Distribution of "Landau" hysterons

In our model, the distribution of "Landau" hysterons is described by a function $\mathcal{L}_\alpha(\alpha)\mathcal{L}_\beta(\beta)\mathcal{L}_{int}(E_{int})$. Here we discuss the characteristics of $\mathcal{L}_\alpha(\alpha)$, $\mathcal{L}_\beta(\beta)$ and

$\mathcal{L}_{int}(E_{int})$.

Recall α_0 and β are positive. Also, α is taken as $\alpha_0(T_c - T)$ in the Landau theory. Thus, α in $\mathcal{L}_\alpha(\alpha)$ and β in $\mathcal{L}_\beta(\beta)$ may range between 0 and ∞. We assume $\mathcal{L}_\alpha(\alpha)$ and $\mathcal{L}_\beta(\beta)$ are functions with a single peak, such as log-normal functions. Their means may be taken as the Landau parameters α_0 and β calculated from experiment in the usual way, and their standard deviations by fitting the experimental *D-E* curves. From observations of real materials, the *D-E* hysteresis major ascending and descending curves are anti-symmetric about the origin of the *D-E* plane. Since the electric displacement of the material is the sum of the μ's of hysterons, $\mathcal{L}_{int}(E_{int})$ should be an even function with a single peak and zero mean, such as a normal distribution function.

Based on the Landau theory, α in a Landau hysteron changes with temperature, so the distribution of α is temperature dependent. From experiments, temperature T linearly affects α. Consider a reference temperature $\theta < T_c$, and let $\alpha_\theta = \alpha_0(T_c - \theta)$ and $\mathcal{L}_\alpha(\alpha_\theta)$ be the distribution of α at θ. When the temperature changes to $T < T_c$, let $\alpha_T = \alpha_0(T_c - T)$ and $\mathcal{L}_\alpha'(\alpha_T)$ be the distribution of α at T. We define J to be the absolute value of the ratio of α_T to α_θ, i.e.

$$J \equiv \left|\frac{\alpha_T}{\alpha_\theta}\right| = \left|\frac{T_c - T}{T_c - \theta}\right|. \tag{2.21}$$

The relation between $\mathcal{L}_\alpha(\alpha_\theta)$ and $\mathcal{L}_\alpha'(\alpha_T)$ is given by

$$\mathcal{L}_\alpha'(\tilde{\alpha}_T) = \mathcal{L}_\alpha(\alpha_\theta)\frac{d\alpha_\theta}{d\alpha_T} = \frac{1}{J}\mathcal{L}_\alpha\left(\frac{\alpha_T}{J}\right). \tag{2.22}$$

For $T > T_c$, $\alpha_T = \alpha_0(T_c - T) < 0$. Similar to the case of temperature greater than T_c, J is $|(T_c - T)/(T_c - \theta)|$. The relation between $\mathcal{L}_\alpha(\alpha_\theta)$ and $\mathcal{L}_\alpha'(\tilde{\alpha}_T)$ is given by

$$\mathcal{L}_\alpha'(\tilde{\alpha}_T) = \mathcal{L}_\alpha(\alpha_\theta)\frac{d\alpha_\theta}{d\tilde{\alpha}_T} = \frac{1}{J}\mathcal{L}_\alpha\left(\frac{\tilde{\alpha}_T}{J}\right). \tag{2.23}$$

We conclude that if the temperature changes from θ to T, the distribution of α is changed from $\mathcal{L}_\alpha(\alpha_\theta)$ to $\mathcal{L}_\alpha'(\alpha_T)$ for $T < T_c$ or to $\mathcal{L}_\alpha'(\tilde{\alpha}_T)$ for $T > T_c$, and the relation between these two functions are shown in Equations (2.22) and (2.23). Figure 2.3(a) shows an example of the distribution of α with different J's. A larger J means a larger $|T_c - T|$.

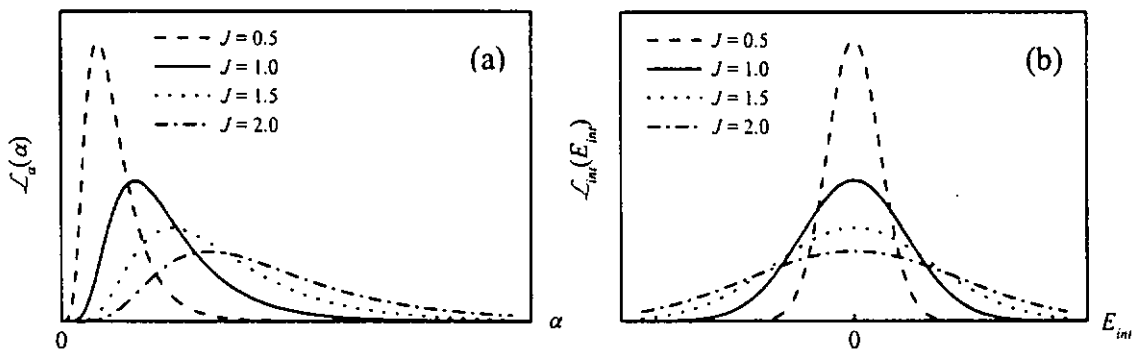

FIG. 2.3 (a) An example of a distribution of α at different J. (b) An example of a distribution of E_{int} at different J. The distribution of α shown is a log-normal function (see Equations (2.22) and (2.26)), and the distribution of E_{int} is a normal distribution function (see Equations (2.25) and (2.28)).

On the other hand, a change in the distribution of α will lead to a change in the distribution of hysterons (see Equation (2.7)). The interactions among hysterons therefore change with temperature because the electric displacement of hysterons

changes with temperature. Ploss and Heiler [Ploss and Heiler, 1992] reported that a small bias field was observed in the paraelectric phase of triglycine sulfate (TGS) from nonlinear dielectric measurements and the bias field is linearly dependent on temperature. Thus in the present paper, the interaction field E_{int} is assumed to depend linearly on temperature, or more specifically E_{int} is linearly proportional to $T - T_c$. Following a similar method as for the case of α, the absolute value of the ratio of interaction fields E_{int} at T and θ is

$$\left|\frac{E_{int}(T)}{E_{int}(\theta)}\right| = \left|\frac{T - T_c}{\theta - T_c}\right| = J. \tag{2.24}$$

The relation between $\mathcal{L}_{int}(E_{int}(\theta))$ and $\mathcal{L}_{int}'(E_{int}(T))$ is given by

$$\mathcal{L}_{int}'(E_{int}(T)) = \mathcal{L}_{int}(E_{int}(\theta))\frac{dE_{int}(\theta)}{dE_{int}(T)} = \frac{1}{J}\mathcal{L}_{int}\left(\frac{E_{int}(T)}{J}\right). \tag{2.25}$$

For a reference temperature θ, the distribution of E_{int} is changed from $\mathcal{L}_{int}(E_{int}(\theta))$ to $\mathcal{L}_{int}'(E_{int}(T))$ if temperature changes to T. Also, the relation between these two functions is shown in Equation (2.25). We remark that the "J" for α and the "J" for E_{int} turn out to be identical functions of T as a result of our simple choice for the temperature dependence of E_{int}. Figure 2.3(b) shows an example of the distribution of E_{int} with different J's. Again a larger J means a larger $|T_c - T|$.

2.3 Deletion and Other Properties of Preisach-Landau model

Since our model encompasses the key concepts of the Preisach model, it can

describe minor loops of a ferroelectric which the Landau theory cannot. As stated earlier, the deletion property and the congruency property characterize the classical Preisach model (see Chapter 1). This section will discuss whether such properties are retained in our model for temperature $T < T_c$. Also, the property of equal vertical chords of the classical Preisach model is introduced.

2.3.1 Deletion property

To show the deletion property, it is necessary to consider a field history as shown in Figure 2.4. In Figure 2.4(a), applied fields a_1, a_2, b_1 are extrema. If the electric displacement of the model at time t_2 is the same as at time t_4, then the deletion property exists because the effect of local extrema a_2 and b_1 are wiped out, i.e. local extrema a_2 and b_1 may be omitted from the sequence of the applied fields. It is also true if the roles of minima and maxima are interchanged.

Figure 2.4(b) shows that after applying the field b_1, the E_{crit}-E_{int} plane (or U-V plane) is divided into three parts: S^+, S^- and O. Each hysteron in S^+ is at the "switch-up" state, and each hysteron in S^- is at the "switch-down" state. Note that the state of hysterons in O is not changed after applying the fields a_1 and b_1. In Figure 2.4(c), the plane after applying the field a_2 is divided into four parts: R, S^+, S^- and O. Comparing with Figure 2.4(b), S^+ is reduced by R after applying a_2, and R is a triangular region where each

hysteron in S^- is at the "switch-down" state. After that, the applied field increases again. When the time is t_4, the applied field will be equal to b_1. The distribution of S^+, S^- and O in the plane (Figure 2.4(d)) is the same as that in Figure 2.4(b). Thus, the electric displacement at t_4 and at t_2 should be the same. It means that the effect of a_2 is wiped out. Therefore, the deletion property exits.

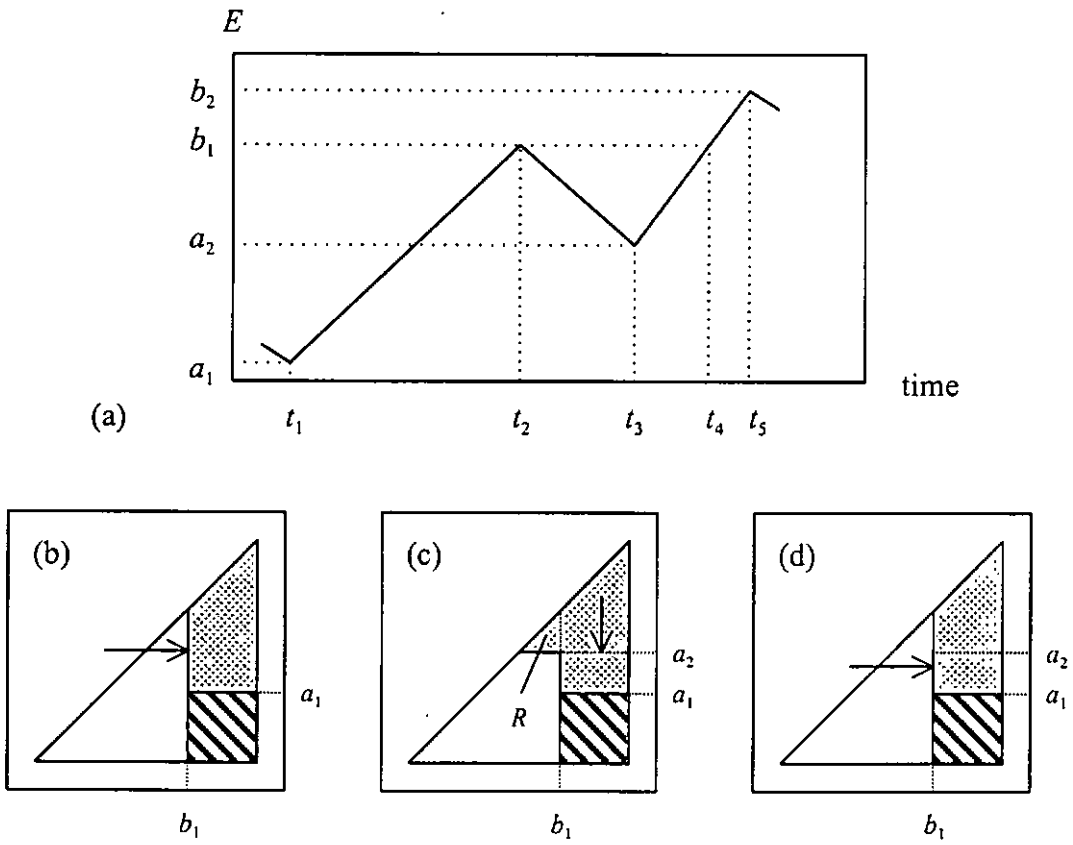

FIG. 2.4 (a) Sequence of applied fields. The corresponding status of the Preisach plane at time (b) t_2, (c) t_3 and (d) t_4. The white, gray and shaded regions in the E_{crit}-E_{int} plane denote the regions S^+, S^- and O respectively.

2.3.2 Congruency property

In our model, the congruency property does not exist. The following illustrates this fact. Consider distributions of α, β and E_{int} given by

$$\mathcal{L}_{\alpha}(\alpha) = \frac{\bar{\alpha}}{\sqrt{2\pi}\alpha\sigma_{\alpha}} \exp\left[-\frac{\ln^2(\alpha/\bar{\alpha})}{2(\sigma_{\alpha}/\bar{\alpha})^2}\right]; \tag{2.26}$$

$$\mathcal{L}_{\beta}(\beta) = \frac{\bar{\beta}}{\sqrt{2\pi}\beta\sigma_{\beta}} \exp\left[-\frac{\ln^2(\beta/\bar{\beta})}{2(\sigma_{\beta}/\bar{\beta})^2}\right]; \tag{2.27}$$

$$\mathcal{L}_{int}(E_{int}) = \frac{1}{\sqrt{2\pi}\sigma_{int}} \exp\left[-\frac{1}{2}\left(\frac{E_{int}}{\sigma_{int}}\right)^2\right]. \tag{2.28}$$

Table 2.1 shows the values of the parameters used. Three simulated minor loops between the same pair of fields are generated by applied fields shown in Figure 2.5. The first minor loop is traced from points 1 to 3, the second from points 4 to 6 and the third from points 7 to 9. Figure 2.6(a) displays the corresponding *D-E* minor loops. It is seen from Figure 2.6(b) that these minor loops are not congruent. This means the model does not have the congruency property of the classical Preisach.

TABLE 2.1 The parameters of the distributions of α, β, and E_{int} used in the simulation.

$\bar{\alpha}$ (10^6 Vm/C)	σ_{α} (10^6 Vm/C)	$\bar{\beta}$ (10^{10} Vm^5/C^3)	σ_{β} (10^{10} Vm^5/C^3)	σ_{int} (10 V/cm)
312.3	20	91.43	40	300

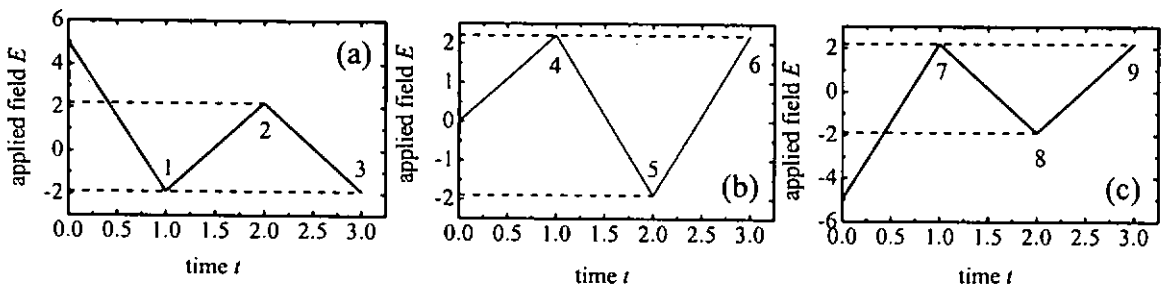

FIG. 2.5 The sequence of applied fields for tracing (a) an upper loop, (b) a middle loop and (c) a lower loop.

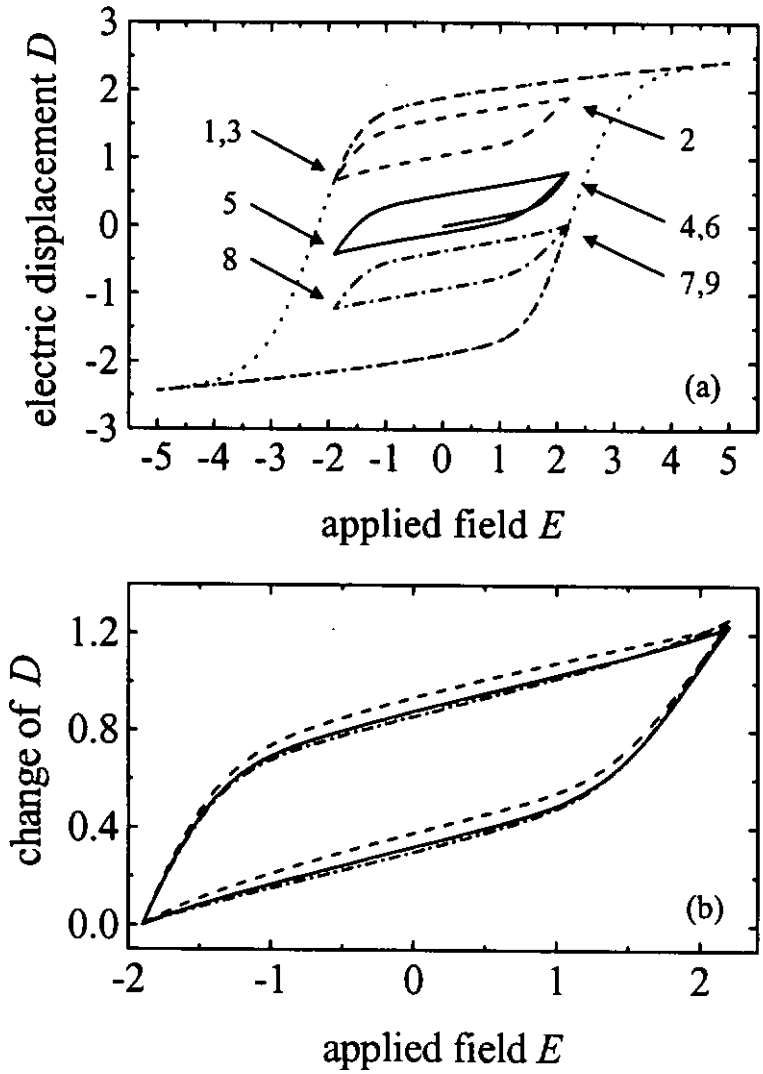

FIG. 2.6 (– – – –), (———) and (–·–·–) denote upper, middle and lower loops respectively. (a) The *D-E* curves and (b) the change of *D* curves when the sequence of fields as shown in Figure 2.5 is applied. The three loops are not congruent. Also shown in (a) is the major loop of the material.

2.3.3 Property of equal vertical chords

In many modifications of the classical Preisach model [Mayergoyz, 1991], the congruency property does not hold. However, in some of these, such as the moving Preisach model, the deletion property as well as the property of equal vertical chords are

still preserved. The property of equal vertical chords may be stated as follows. Consider a minor loop between a pair of external fields E_0 and E_1 (Figure 2.7(a)). For an applied field E within the range E_0 and E_1, let $D_{upper}(E)$ and $D_{lower}(E)$ be the electric displacement corresponding to the upper and lower branches of this minor loop. $D_{upper}(E) - D_{lower}(E)$ is the vertical chord at E for the minor loop. The property of equal vertical chords states that the chords $D_{upper}(E) - D_{lower}(E)$ evaluated at E are the same for all minor loops between fields E_0 and E_1. In the following, this property is proved in our model.

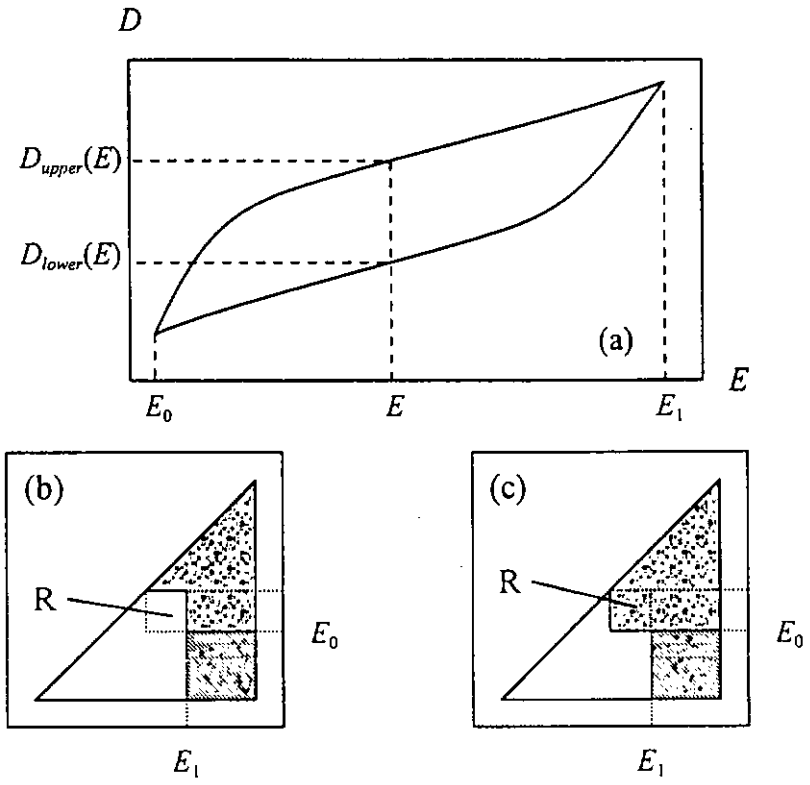

FIG. 2.7 (a) A minor loop formed between E_0 and E_1. The distribution of hysterons on the Preisach plane corresponding to an applied field E and electric displacement (b) $D_{upper}(E)$ and (c) $D_{lower}(E)$. The white, gray and shaded regions in the E_{crit}-E_{int} plane denote the regions S^+, S^- and O respectively.

From Figures 2.7(b) and (c), it is seen that the E_{crit}-E_{int} plane (or U-V plane) is divided into four parts: R, S^+, S^- and O. Each hysteron in S^+ is at the "switch-up" state, and each hysteron in S^- is at the "switch-down" state. Note that the state of hysterons in O is not changed after applying the fields E_0 and E_1. In the region R, the state of hysterons is in the "up" or "down" state if the applied field E ($E_0 \le E \le E_1$) is a decreasing field or increasing field respectively. Thus,

$$D_{upper}(E) - D_{lower}(E) = \iint_R \frac{2}{\sqrt{3}} \cos\left[\frac{1}{3}\cos^{-1}\left(\frac{E - E_{int}}{E_{crit}}\right)\right] \mathcal{L}_{crit}\mathcal{L}_{int}\, dE_{int}dE_{crit} - \iint_R \frac{2}{\sqrt{3}} \cos\left[\frac{1}{3}\cos^{-1}\left(\frac{E - E_{int}}{E_{crit}}\right) + \frac{2\pi}{3}\right] \mathcal{L}_{crit}\mathcal{L}_{int}\, dE_{int}dE_{crit} \tag{2.29}$$

Since the region R is bounded by the fields E, E_0 and E_1 only, $D_{upper}(E) - D_{lower}(E)$ is not affected by the past field history. This proves that all minor loops between E_0 and E_1 have equal vertical chords at the same field E.

2.4 Comparison of the model with Landau theory

The Landau theory has been successful in explaining the thermodynamic properties of ferroelectrics near T_c. In our model, all the broad features of the thermodynamic properties of the Landau theory are retained. To illustrate this claim, we use an example to discuss remanent polarization, coercive field and dielectric constant of a "second

order" material by our model.

The material chosen is triglycine sulfate (TGS), with Curie temperature $T_c = 49.5\,°\mathrm{C}$. Gaffar *et al.* [Gaffar *et al.*, 1989] measured the dielectric constant ε_r and the remanent polarization P_r at different temperatures. Using these results, the Landau parameter α_0 is determined by the slope of the $1/\varepsilon_r(T)$ curve, which gives $\alpha_0 = 32.87\times10^6$ Vm/C/K. By a least squares fitting of the $P_r(T)$ curve, the Landau parameter β is found to be 91.43×10^{10} Vm^5/C^3. The distributions of α, β and E_{int} at reference temperature $\theta = 40°\mathrm{C}$ are assumed to be the distributions shown in Equations (2.26)-(2.28), with parameters given in Table 2.1. Using these parameters, the *D-E* major loops at different temperatures are simulated (Figure 2.8). It is seen that as the temperature increases, the major loop becomes thinner, and the coercive field and remanent polarization decrease in magnitude. When the temperature increases to a value larger than T_c, the *D-E* relation becomes non-hysteretic. Here, in the low field region, a linear *D-E* relation exists. As the temperature continues to increase, the *D-E* curve becomes flatter, and the linear *D-E* region expands. When temperature is large enough, the whole *D-E* curve almost becomes a straight line. Compared with the Landau theory, our model can produce more realistic *D-E* loops than Landau's, because now there is no discontinuous jump between the up and down states.

Figures 2.9-2.11 show the variation of remanent polarization, coercive field and

reciprocal dielectric constant with temperature. The Landau theory shows that remanent polarization is directly proportional to $\sqrt{T_c - T}$, and coercive field is directly proportional to $(T_c - T)^{3/2}$, and reciprocal dielectric constant is a V-shaped curve. These broad features are reproduced by our model. In fact that the Landau theory is a special case of our model without the distribution of hysterons. In our model, a material is considered to be a collection of hysterons so that all properties of the material are dependent on the properties and the distribution of the hysterons. Hysterons with different critical fields and remanent polarizations combine to give the properties of the whole material. Thus it is remarkable to see that the temperature dependence of these two properties as well as dielectric constant can still come out close to that of the Landau theory, preserving the power of the latter.

Comparing with the experimental results [Gaffar *et al.*, 1989], the Landau theory and simulations based on our model give remanent polarizations very close to the measured data (Figure 2.9). In Figure 2.10, the temperature dependence of the coercive field is simulated. Although the simulation of the present model is very close to the result obtained from the Landau theory, these predictions are two order of magnitude larger than the experimental values (which is well known for the Landau theory). For the reciprocal dielectric constant (Figure 2.11) in the paraelectric phase ($T > T_c$), both of the predictions are in good agreement with the experiment. In the ferroelectric phase

($T < T_c$), both of the predictions show the broad feature of the experimental curve, i.e. more or less a straight line. But, in vicinity of T_c, both predictions cannot reproduce the fine features. In particular, a finite value of the reciprocal dielectric constant at T_c is not obtained. (A modification of the model presented in this section, which can produce a finite value of $1/\varepsilon_r(T_c)$, will be introduced in next section).

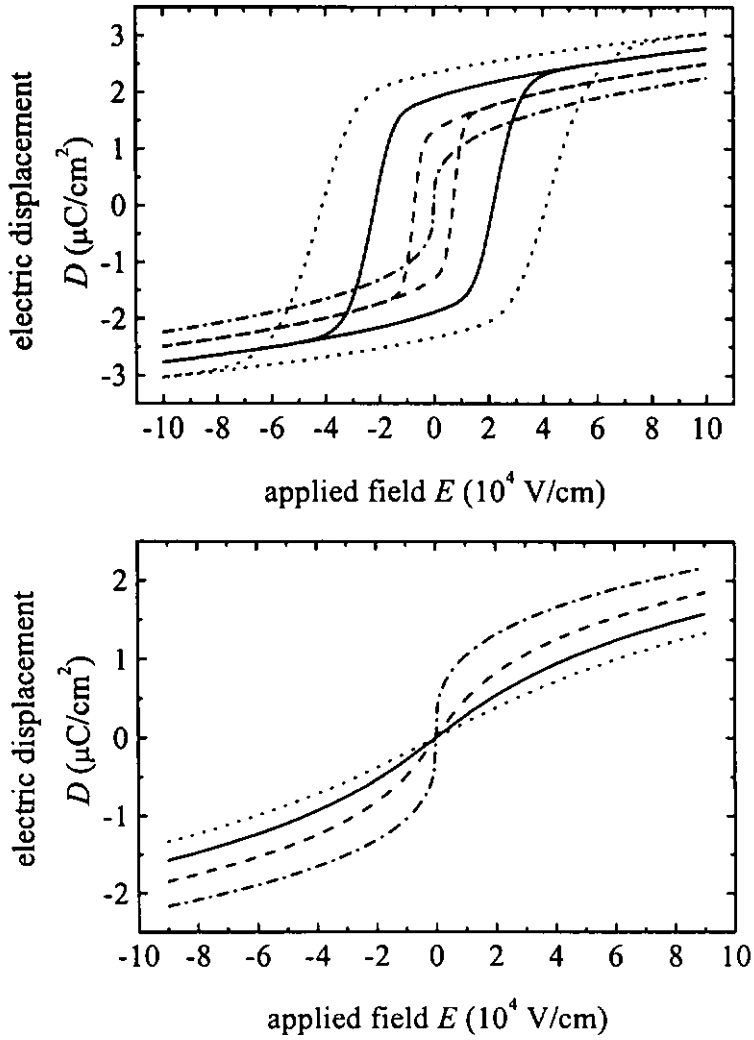

FIG. 2.8 The *D-E* relation at different temperatures *T* of TGS (Section 2.4). (a) (·····), (——), (– –) and (— ·) denote the *D-E* loops at $T = 35$ °C, θ, 45 °C and T_c respectively. (b) (·····), (——), (– –) and (— ·) denote the *D-E* curves at T = 65 °C, 60 °C, 55 °C and T_c respectively.

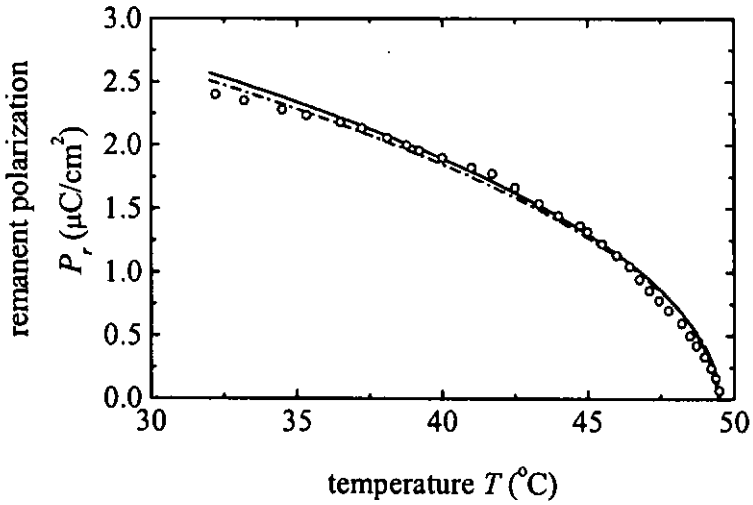

FIG. 2.9 The variation of remanent polarization P_r with temperature $T < T_c$ of TGS (Section 2.4). The solid and dash-dotted lines are calculated from our model and the Landau theory respectively. The circles denote the experimental results [Gaffar *et al.*, 1989].

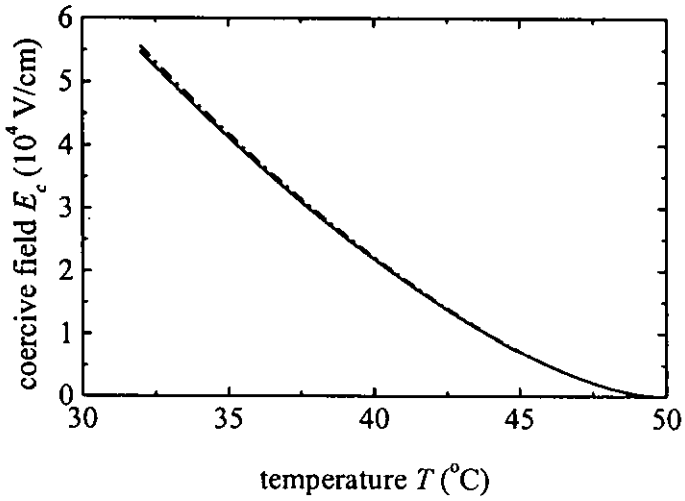

FIG. 2.10 The variation of coercive field E_c with temperature $T < T_c$ of TGS (Section 2.4). The solid and dash-dotted lines are calculated from our model and the Landau theory respectively.

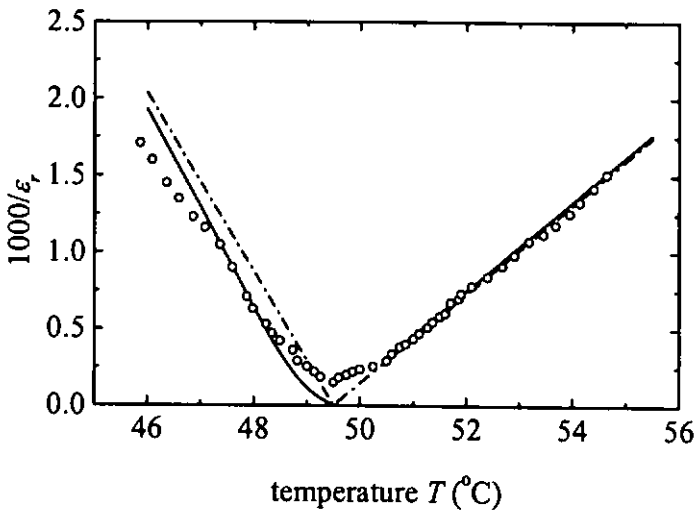

FIG. 2.11 The variation of the reciprocal dielectric constant with temperature T of TGS (Section 2.4). The solid and dash-dotted lines are calculated from our model and the Landau theory respectively. The circles denote the experimental results [Gaffar *et al.*, 1989].

2.5 Modified Preisach-Landau model

In the study of triglycine sulfate (TGS), it is observed in many investigations that the dielectric constant ε_r has a finite value at the phase transition temperature T_c [Craig, 1966; Chincholkar and Unruh, 1968; Mansingh and Eswar Prasad, 1977]. In this section, a more refined Preisach-Landau model is proposed to tackle features such as finite dielectric constant at T_c. A Preisach-Landau material (see Section 2.2) consists of a collection of Landau hysterons. Each hysteron is described by three parameters: α, β and E_{int}. Thus the distribution of hysterons (or the distributions of α, β and E_{int}) characterizes the ferroelectric material. Here we propose to express the interaction field E_{int} as $E_{int} = k_{10}(T_c - T) + k_0$ where k_0 and k_{10} are real numbers with a distribution (in Section 2.2, $k_0 = 0$) so that E_{int} may not be zero at T_c and a finite dielectric constant at

T_c is obtained. Comparing with the experimental results of Gaffar *et al.* [Gaffar *et al.*, 1989], this modification produces a finite reciprocal dielectric constant at the phase transition temperature but the model in Section 2.2 cannot. Also, this modification is able to account for finer features of the experimental $1/\varepsilon_r$-T curve.

2.5.1 The modified model

Ploss and Heiler [Ploss and Heiler, 1992] reported that a small bias field was observed in the paraelectric phase of triglycine sulfate (TGS) from nonlinear dielectric measurements and the bias field is linearly dependent on temperature. The interaction field E_{int} is therefore written as $E_{int} = k_1 + k_0$ where $k_1 = k_{10}(T - T_c)$. k_0 and k_{10} may range between $-\infty$ and $+\infty$ (in Section 2.2, we only assumed $E_{int} = k_{10}(T - T_c)$ in the interest of simplicity). Thus, for $T \neq T_c$, the distribution of E_{int} is

$$\begin{aligned}\mathcal{L}_{int}(E_{int}) &= \int_{-\infty}^{\infty} \mathcal{L}_{k_0}(E_{int} - k_1)\mathcal{L}_{k_1}(k_1)dk_1 \\ &= \int_{-\infty}^{\infty} \mathcal{L}_{k_0}(E_{int} - k_{10}(T - T_c))\mathcal{L}_{k_{10}}(k_{10})dk_{10} \qquad (2.30)\end{aligned}$$

where $\mathcal{L}_{k_0}(k_0)$ and $\mathcal{L}_{k_1}(k_1)$ are the distribution functions for k_0 and k_1 respectively. At $T = T_c$, $E_{int} = k_0$ and the distribution of E_{int} is given by

$$\mathcal{L}_{int}(E_{int}) = \mathcal{L}_{k_0}(k_0). \qquad (2.31)$$

According to $\alpha = \alpha_0(T_c - T)$, $\alpha = 0$. Thus, the μ of a hysteron becomes $((E - E_{int})/\beta)^{1/3}$ and the distribution of Landau hysterons becomes

$\mathcal{L}(\beta, E_{int}) = \mathcal{L}_{\beta}(\beta)\mathcal{L}_{int}(E_{int})$. The electric displacement of the material at T_c is

$$D(E) = \int_0^{\infty}\int_{-\infty}^{\infty}\left(\frac{E - E_{int}}{\beta}\right)^{1/3} \mathcal{L}_{int}(E_{int})\mathcal{L}_{\beta}(\beta)\, dE_{int} d\beta . \tag{2.32}$$

Since $\mu(E)$ is non-hysteretic at T_c, the permittivity of the material is

$$\varepsilon(E) = \int_0^{\infty}\int_{-\infty}^{\infty}\frac{\partial}{\partial E}\left[\left(\frac{E - E_{int}}{\beta}\right)^{1/3}\right]\mathcal{L}_{int}(E_{int})\mathcal{L}_{\beta}(\beta)\, dE_{int} d\beta \tag{2.33}$$

From experimental observations of real materials, the *D-E* hysteresis major ascending and descending curves are anti-symmetric about the origin of the *D-E* plane. Since the electric displacement of the material is the sum of the μ's of hysterons, $\mathcal{L}_{k_0}(k_0)$ and $\mathcal{L}_{k_1}(k_1)$ (or $\mathcal{L}_{k_{10}}(k_{10})$) should be an even function with a single peak (say) and zero mean, such as a normal distribution function. $\mathcal{L}_{int}(E_{int})$ is then an even function with a single peak and zero mean (using Equations (2.30) and (2.31)). Following a similar method as for the case of α, the distribution of k_1 at $T \neq T_c$ is

$$\mathcal{L}_{k_1}'(k_1(T)) = \mathcal{L}_{k_1}(k_1(\theta))\frac{dk_1(\theta)}{dk_1(T)} = \frac{1}{J}\mathcal{L}_{k_1}\left(\frac{k_1(T)}{J}\right) \tag{2.34}$$

and the distribution of E_{int} at $T \neq T_c$ is

$$\mathcal{L}_{int}'(E_{int}(T)) = \int_{-\infty}^{\infty}\mathcal{L}_{k_0}(E_{int}(T) - k_1(T))\mathcal{L}_{k_1}'(k_1(T))dk_1(T) . \tag{2.35}$$

We conclude that after modifying the Preisach-Landau model of Section 2.2, the distribution of E_{int} at different temperature T is now described by Equations (2.31) and (2.35) (i.e. Equation (2.25) is replaced by Equations (2.31) at $T = T_c$ and (2.35) at $T \neq T_c$).

2.5.2 Comparison with experimental data

Gaffar *et al.* [Gaffar *et al.*, 1989] measured the dielectric constant ε_r at zero field and the remanent polarization P_r of triglycine sulfate (TGS) at temperatures around its Curie temperature T_c of 49.5 °C. In Section 2.4, the data from Gaffar *et al.* were chosen as an example to demonstrate the viability of the Preisach-Landau model with $k_0 = 0$. The Curie temperature T_c in the model was taken as 49.5 °C. The distributions of α and β at reference temperature $\theta = 40°C$ were assumed to be given by Equations (2.26) and (2.27) respectively. The distribution of E_{int} at θ was assumed to be Equation (2.28). The parameters of these distributions are shown in Table 2.2. Figures 2.12 and 2.13 show the simulated reciprocal dielectric constant $1/\varepsilon_r$ and simulated remanent polarization P_r at different temperatures. In the refined model ($k_0 \neq 0$) described in this section, we take the Curie temperature T_c as 49.8 °C, and the distributions of α and β at reference temperature $\theta = 40°C$ are assumed to be given by Equations (2.26) and (2.27) respectively while the distributions of k_0 and k_1 at θ are given by

$$\mathcal{L}_{k_0}(k_0) = \frac{1}{\sqrt{2\pi}\,\sigma_{k_0}} \exp\left[-\frac{1}{2}\left(\frac{k_0}{\sigma_{k_0}}\right)^2\right]; \tag{2.36}$$

$$\mathcal{L}_{k_1}(k_1) = \frac{1}{\sqrt{2\pi}\,\sigma_{k_1}} \exp\left[-\frac{1}{2}\left(\frac{k_1}{\sigma_{k_1}}\right)^2\right]. \tag{2.37}$$

The parameters used for the present calculations are shown in Table 2.2. Using

these parameters the reciprocal dielectric constant $1/\varepsilon_r$ and the remanent polarization P_r at different temperatures are calculated and compared, in Figures 2.12 and 2.13, with the results simulated by the Preisach-Landau model in Section 2.2 and the experimental results [Gaffar *et al.*, 1989].

TABLE 2.2 The Curie temperature T_c and the parameters of the distributions of α, β, k_0 and k_1 at $\theta = 40°C$ used in the model in Section 2.2 and the present model.

	$\bar{\alpha}$ (10^6 Vm/C)	σ_α (10^6 Vm/C)	$\bar{\beta}$ (10^{10} Vm^5/C^3)	σ_β (10^{10} Vm^5/C^3)
model in Section 2.2	312.3	20	91.43	40
present model	334.1	20	99.64	70
	σ_{int} (10 V/cm)	σ_{k_0} (10 V/cm)	σ_{k_1} (10 V/cm)	T_c (°C)
model in Section 2.2	300	—	—	49.5
present model	—	50	400	49.8

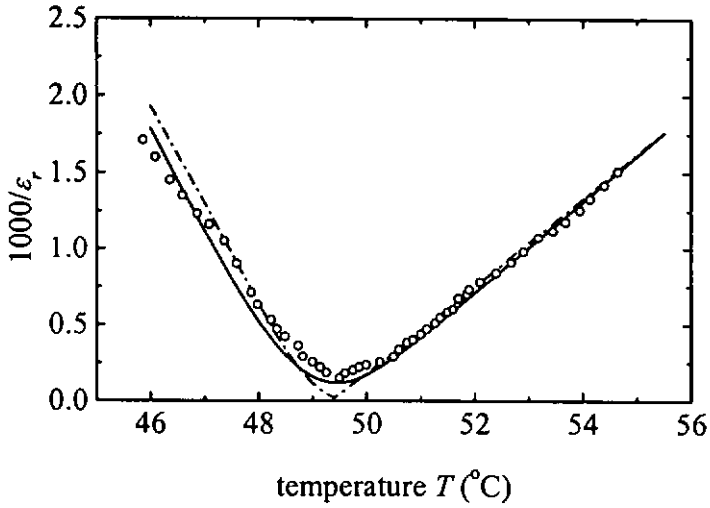

FIG. 2.12 The variation of the reciprocal dielectric constant with temperature T of TGS. The solid and dash-dotted lines are calculated from the present model and a Preisach-Landau model in Section 2.2 respectively. The circles denote the experimental results [Gaffar *et al.*, 1989].

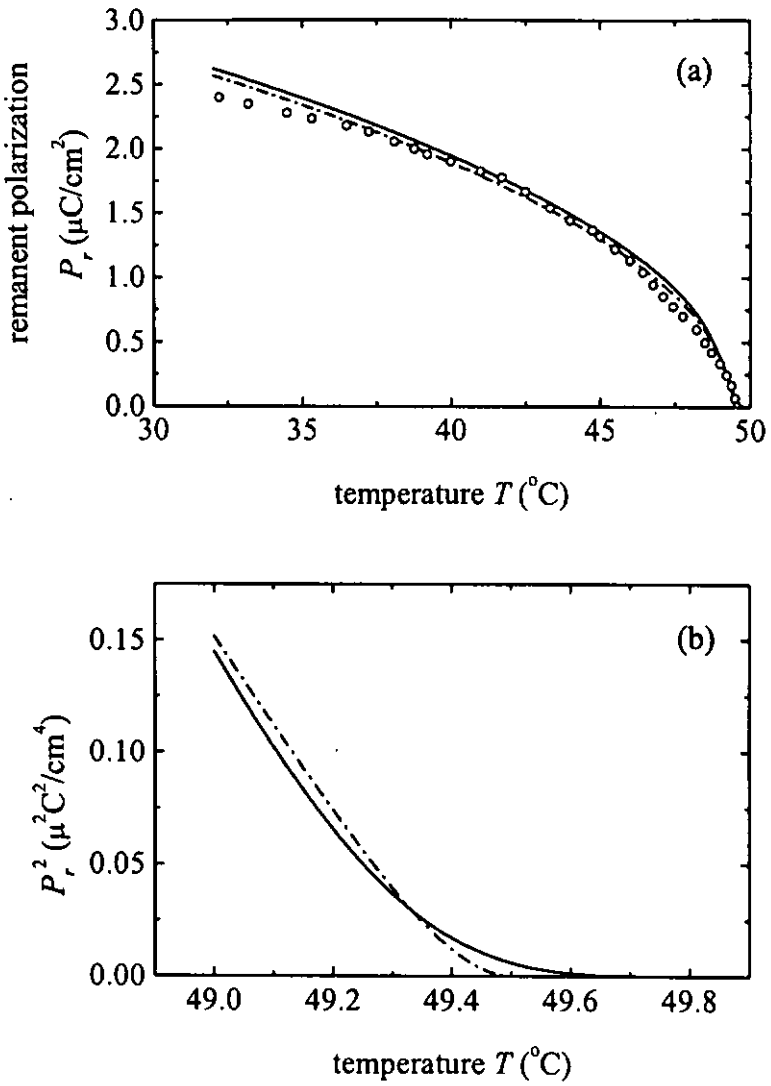

FIG. 2.13 (a) The variation of the remanent polarization with temperature T of TGS. (b) The P_r^2-T curve in the vicinity of T_c. The solid and dash-dotted lines are calculated from the present model and the Preisach-Landau model in Section 2.2 respectively. The circles denote the experimental results [Gaffar *et al.*, 1989].

From Figure 2.12, it is seen that the $1/\varepsilon_r$-T curve simulated by the Preisach-Landau model in Section 2.2 is V-shaped. This matches the broad features of the experimental curve and the prediction of the Landau theory. However, the simulated $\varepsilon_r(T_c)$ has an infinite value (same result obtains from Landau theory), which contradicts the experimental observation. This discrepancy is related to the limitation that, at the

Curie point, all hysterons do not shift along the E-axis ($E_{int} = 0$ at T_c). Therefore, the electric displacement of each hysteron has the form $(E/\beta)^{1/3}$ at T_c. It is clear that its reciprocal dielectric constant at zero field is zero. Since the permittivity of the whole material is the sum of the permittivity of each hysteron (see Equation (2.33)), the reciprocal dielectric constant of the whole material is zero.

On the other hand, the present model obtains a finite $\varepsilon_r(T_c)$. The reason is that the interaction field is written as $E_{int} = k_{10}(T_c - T) + k_0$ so that the dielectric constant at T_c is finite according to Equations (2.31) and (2.33). In addition, Figure 2.12 shows that, in the region near T_c, the slope of the experimental $1/\varepsilon_r$-T curve decreases gradually as the temperature T tends to T_c. This profile can be reproduced by the present model, and a good agreement with the experiment is obtained. We know that the distribution of Landau hysterons changes with temperature. According to Equations (2.22), (2.23) and (2.35), the change in the distribution of Landau hysterons decreases gradually as temperature T tends to T_c. Therefore, from Equations (2.15), (2.17), (2.20) and (2.33), the simulated $1/\varepsilon_r$-T curve can cope with the experimental curve.

Figure 2.13(a) shows the variation of the remanent polarization P_r with temperature T calculated by both models. The two simulated curves agree well with the experiment. We see that, in Figure 2.13(b), the P_r^2-T curve simulated by the present model has a tail in the vicinity of T_c, while the curve simulated by the model of Section

2.2 has not noticeable tail. In the experimental literature, this tail had been observed [Deguchi and Nakamura, 1972; Ehses and Schmitt, 1978].

Chapter 3

Nonlinear dielectricity of ferroelectrics

3.1 Introduction

Due to the property that the polarization is non-zero at zero field in a ferroelectric, ferroelectric materials become useful as switchable devices, especially computer memories. However, because of nonlinear and "history" dependent effects a ferroelectric material does not exhibit "well-defined" behavior so that care must taken in more delicate applications. For example, in ferroelectric memories [Scott and Paz de Araujo, 1989], a transistor is added to each ferroelectric cell for isolation from one another to avoid the influence of "history" effect. Many applications, such as precision machining, require that ferroelectrics can be operated in high stress and high electric field. However, pronounced nonlinear dielectric properties and hysteresis behavior are evident in these conditions. For these and other reasons, there have been many researches on the nonlinear dielectricity of ferroelectric materials. One traditional approach is to write the electric displacement or polarization as a Taylor series of electric field. The disadvantage is that this approximation is only adequate in the low field range. For instance, Taylor and Damjanovic [Taylor and Damjanovic, 1998] reported that the amplitude and phase

angle of the first and third harmonic determined from minor polarization loops could not be predicted adequately by this approach, one reason being that the maximum field amplitudes considered were quite close to the coercive field of the material.

In another approach, some investigators use the Preisach model in the study of nonlinearity and hysteresis of ferroelectrics. Hughes and Wen [Hughes and Wen, 1997] applied the Preisach model to research hysteretic behavior of piezoceramics and shape memory alloys. Hall [Hall, 2001] mentioned that the Preisach model have been successfully employed in piezoelectric ceramics. In this chapter, we attempt to study the *D-E* loops of a ferroelectric material, measured under sinusoidal electric field excitation, by two models, Preisach model and Preisach-Landau model, and analyze both the in-phase and out-of-phase components of D by Fourier transform to obtain nonlinear dielectricity information. Polyvinylidene fluoride (PVDF) is chosen as an example for this study. The resulting Fourier coefficients are compared to the experimental data given by Furukawa *et al.* [Furukawa *et al.*, 1987]. The predictions of both models are able to reproduce almost all the essential experimental features, and are close to each other.

3.2 Methodology

3.2.1 Methodology based on the Preisach model

In this work, the electric displacement $D(E)$ of a ferroelectric is written as $P+\varepsilon E$,

where P, ε, E are polarization, permittivity and field respectively. Clearly, ε may be determined from the slope of the D-E relation in the "saturation" region where $P=P_s$ (see Figure 3.1).

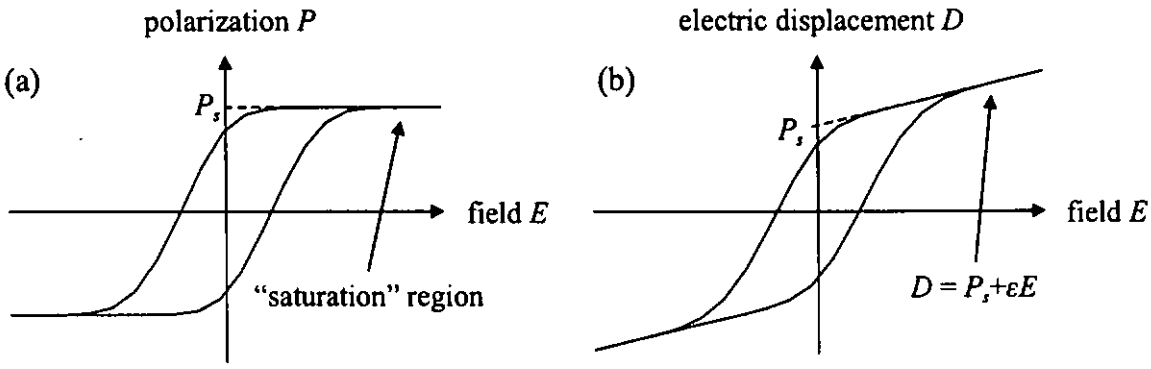

FIG. 3.1 (a) A major (or saturated) P-E hysteresis loop of a ferroelectric. (b) A major D-E hysteresis loop of a ferroelectric with $D = P_s+\varepsilon E$.

Suppose a sinusoidal field $E(t) = E_0 \cos(\omega t)$ is applied on this nonlinear material. Using the Fourier transform techniques, the polarization P and the electric displacement D of a nonlinear dielectric can be expressed as

$$P(t) = P_0 + \sum_{n=1}^{\infty}\left[P_n'\cos(n\omega t) + P_n''\sin(n\omega t)\right] \tag{3.1}$$

$$D(t) = D_0 + \sum_{n=1}^{\infty}\left[D_n'\cos(n\omega t) + D_n''\sin(n\omega t)\right] \tag{3.2}$$

where P_0 and D_0 are constants, and P_n' and P_n'' are the n-th order Fourier coefficients of $P(t)$, and D_n' and D_n'' are the n-th order Fourier coefficients of $D(t)$. Since $D(t) = P(t) + \varepsilon E(t)$, the electric displacement is

$$D(t) = P_0 + (\varepsilon E_0 + P_1')\cos(\omega t) + P_1''\sin(\omega t) + \sum_{n=2}^{\infty}\left[P_n'\cos(n\omega t) + P_n''\sin(n\omega t)\right].$$

(3.3)

Comparing Equation (3.3) with Equation (3.2), we have

$$\begin{cases} D_0 = P_0 \\ D_1' = \varepsilon E_0 + P_1' \\ D_j'' = P_j'' \end{cases} \quad \text{and} \quad D_i' = P_i' \tag{3.4}$$

where $i \geq 2$ and $j \geq 1$. Note that the Preisach model can describe major as well as minor loops [Della Torre, 1999]. So, the *P-E* loops of the material corresponding to sinusoidal excitations of different amplitudes can be calculated by using the Preisach model, and the Fourier coefficients of $D(t)$ can be analyzed by using Equation (3.4). The $D_n'(E_0)$ and $D_n''(E_0)$ curves therefore can be simulated.

In this work, the Preisach function is divided into two components: irreversible and reversible components, i.e.

$$\mathcal{P}(E_{crit}, E_{int}) = \mathcal{P}_{irr}(E_{crit}, E_{int}) + \mathcal{P}_{rev}(E_{crit}, E_{int}). \tag{3.5}$$

The irreversible Preisach function $\mathcal{P}_{irr}(E_{crit}, E_{int})$ is assumed to be the product of a distribution of E_{crit} and a distribution of E_{int} and is given by [Andrei and Stancu, 2000]

$$\mathcal{P}_{irr}(E_{crit}, E_{int}) = SP_s \frac{E_{c0}}{\sqrt{2\pi}\sigma_{crit}E_{crit}} \exp\left[-\frac{\ln^2(E_{crit}/E_{c0})}{2(\sigma_{crit}/E_{c0})^2}\right] \times \frac{1}{\sqrt{2\pi}\sigma_{int}} \exp\left[-\frac{E_{int}^2}{2\sigma_{int}^2}\right] \tag{3.6}$$

where S is the weight of the irreversible component in the total polarization of the material, σ_{int} is the standard deviation of the interaction field, σ_{crit} describes the dispersion of the critical field, and E_{c0} is related to the maximum position of the

distribution of E_{crit}. The reversible Preisach function $\mathcal{P}_{rev}(E)$, which is only defined on the E_{int} axis, is given by [Andrei and Stancu, 2000]

$$\mathcal{P}_{rev}(E) = \frac{(1-S)P_s}{2\sigma_r} \times \exp\left[-\frac{|E|}{\sigma_r}\right] \tag{3.7}$$

where E is the applied field, and σ_r describes the dispersion of the exponential function. In the calculation of the polarization P, we use the Everett integral [Krasnoselskii and Pokrovskii, 1989] defined as

$$\Psi(x,y) = \int_0^{(x-y)/2} \int_{y+E_{crit}}^{x-E_{crit}} \mathcal{P}_{irr}(E_{crit}, E_{int}) dE_{int} dE_{crit} + \int_y^x \mathcal{P}_{rev}(E) dE \tag{3.8}$$

Consider a minor loop between the same pair of fields E_0, $-E_0$. The polarization of the loop at E_0 is

$$P(E_0) = \Psi\big(E_0 + \alpha P(E_0), -E_0 - \alpha P(E_0)\big). \tag{3.9}$$

The descending (P_{down}) and the ascending (P_{up}) branches of the minor loop are given by

$$P_{down}(E) = P(E_0) - 2\Psi\big(E_0 + \alpha P(E_0), E + \alpha P_{down}(E)\big) \tag{3.10}$$

and $$P_{up}(E) = -P(E_0) + 2\Psi\big(E + \alpha P_{up}(E), -E_0 - \alpha P(E_0)\big). \tag{3.11}$$

3.2.2 Methodology based on the Preisach-Landau model

In Section 2.5, a Preisach-Landau model has been introduced. Since this model simulates the D-E relation of a ferroelectric, we can directly and conveniently use the Fourier transform to decompose $D(t)$ to find the $D_n'(E_0)$ and $D_n''(E_0)$. In this simulation, the distribution of Landau hysterons is $L_\alpha(\alpha)L_\beta(\beta)L_{k_0}(k_0)L_{k_1}(k_1)$. The

distribution of α, β, k_0 and k_1 are assumed to be Equations (2.26), (2.27), (2.36) and (2.37) respectively. The electric displacement $D(E)$ of a minor loop is calculated from Equations (2.11) and (2.30).

3.3 Experimental nonlinear dielectricity of PVDF

In the article of Furukawa *et al.* [Furukawa *et al.*, 1987], Furukawa *et al.* investigated the nonlinear dielectricity of PVDF at 20 °C. Minor loops were traced using an electric field with frequency 0.8 Hz. When the field amplitude E_0 was less than 20 MV/m, the *D-E* relation tended to be linear. As the amplitude was increased to values greater than 40 MV/m, the nonlinearity of the *D-E* relation grew, as shown in Figure 3.2 (solid lines). The coercive field E_c of the PVDF was 75 MV/m and its remanent polarization P_r was 60 mC/m^2. Then, these experimental $D(t)$ curves corresponding to different field amplitudes were analyzed by using digital Fourier transforms. The results are shown in Figure 3.3 (open and closed circles).

Furukawa *et al.* proposed a model to explain this behavior. They considered an ideal square *D-E* relation for the material. The displacement D was switched up if the field E was increased to a value greater than the coercive field E_c, and was switched down if the field was decreased to lesser than $-E_c$. Their method is as follows. The phase angle of the electric displacement δ_D is defined as

$$E_0 \sin\delta_D = -E_c, \tag{3.12}$$

where E_0 is the amplitude of E. Using the Fourier transforms, the Fourier coefficients are given by

$$\begin{cases} D_0 = 0; \\ D_n' = (P_r/n)\cos(n\delta_D), & n \geq 1; \\ D_n'' = (P_r/n)\sin(n\delta_D), & n \geq 1. \end{cases} \tag{3.13}$$

The $D_n'(E_0)$ and $D_n''(E_0)$ curves are calculated by using Equations (3.12) and (3.13) with E_c = 75 MV/m and P_r = 60 mC/m^2, as shown in Figure 3.3 (solid and dashed lines).

3.4 Simulations of nonlinear dielectricity of PVDF

The model considered in Furukawa *et al.*'s paper is a square *D-E* hysteresis loop with coercive fields $\pm E_c$ and remanent polarization P_r, where E_c and P_r are obtained from the experimental major loop of the PVDF material. When the amplitude of the applied field, E_0, is varied, the phase angle δ_D of D changes. Using the technique of Fourier analysis, both the in-phase and out-of-phase components of the Fourier coefficients of D are obtained and depend on E_0. Although the predictions of this model are more or less consistent with experiment in the high field range, it cannot describe the nonlinearity behavior at low field, especially $E_0 < E_c$. It is because the coercive field of the square *D-E* hysteresis loop in the model is a constant. If $E_0 < E_c$, then the applied field E is impossible to switch the material and thus δ_D is not well-defined. In the region

near E_c, a sharp change in the Fourier coefficients of D occurs due to the sudden dipolar switch in the model; however, this is not the case in the experiment. Experimentally, a different D-E hysteresis loop is formed for any given amplitude of the applied field, leading to field-dependent P_r and E_c. As a finer point, a fixed P_r value limits $D_1'(E_0)$ to values smaller than P_r, so that in the high field range the predicted $D_1'(E_0)$ comes out to be much smaller than the experimental value.

To understand the behavior of a ferroelectric material under arbitrary field magnitudes it is important to have a model which can describe its major loop as well as D-E histories within. In our simulations, we use the moving Preisach model to simulate D-E loops with different field amplitudes. Table 3.1 shows the Preisach parameters for PVDF fitted from the steady-state major hysteresis loop [Furukawa *et al.*, 1987]. Using these parameters, the simulated D-E curves for the PVDF are compared with the experimental results [Furukawa *et al.*, 1987], as shown in Figure 3.2. From Figure 3.2, we see that for large E_0 the simulated $D(E_0)$ of minor loops are larger than the experimental $D(E_0)$. In the Preisach model, every minor loop generated with field amplitude E_0 must lie inside the major loop, but this is not so strictly true with the experimental data here.

TABLE 3.1 The Preisach parameters and permittivity of PVDF used in the simulation.

E_{c0} (MV/m)	σ_{crit} (MV/m)	σ_{int} (MV/m)	σ_r (MV/m)	α	S	P_s (mC/m^2)	ε (10^{-9}F/m)
69.8	29.9	32.2	67	0.38	0.73	77	0.11[a]

[a] from Furukawa, T., Nakajima, K., Koizumi, T. and Date, M. "Measurements of Nonlinear Dielectricity in Ferroelectric Polymers". *Japanese Journal of Applied Physics*, Part 1 Vol. 26, pp.1039-1045 (1987)

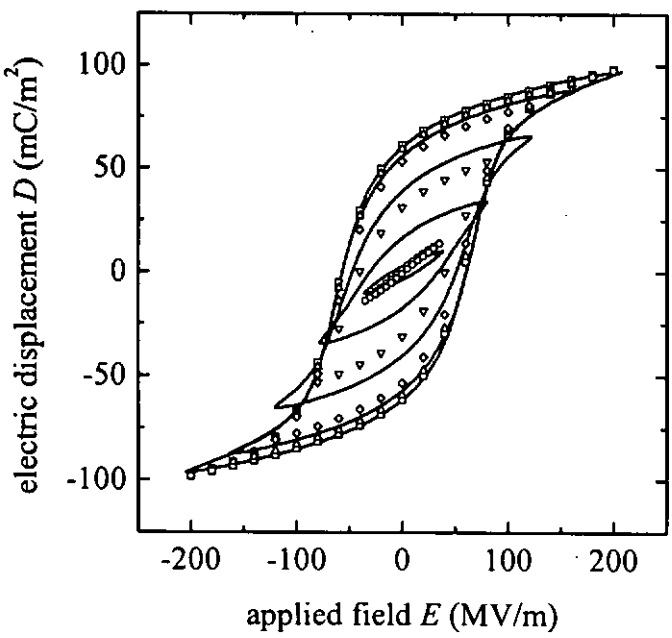

FIG. 3.2 *D-E* loops of PVDF at 20 °C. The simulation results (open symbols) are compared with experimental results in Furukawa *et al.* [Furukawa *et al.*, 1987] (solid lines).

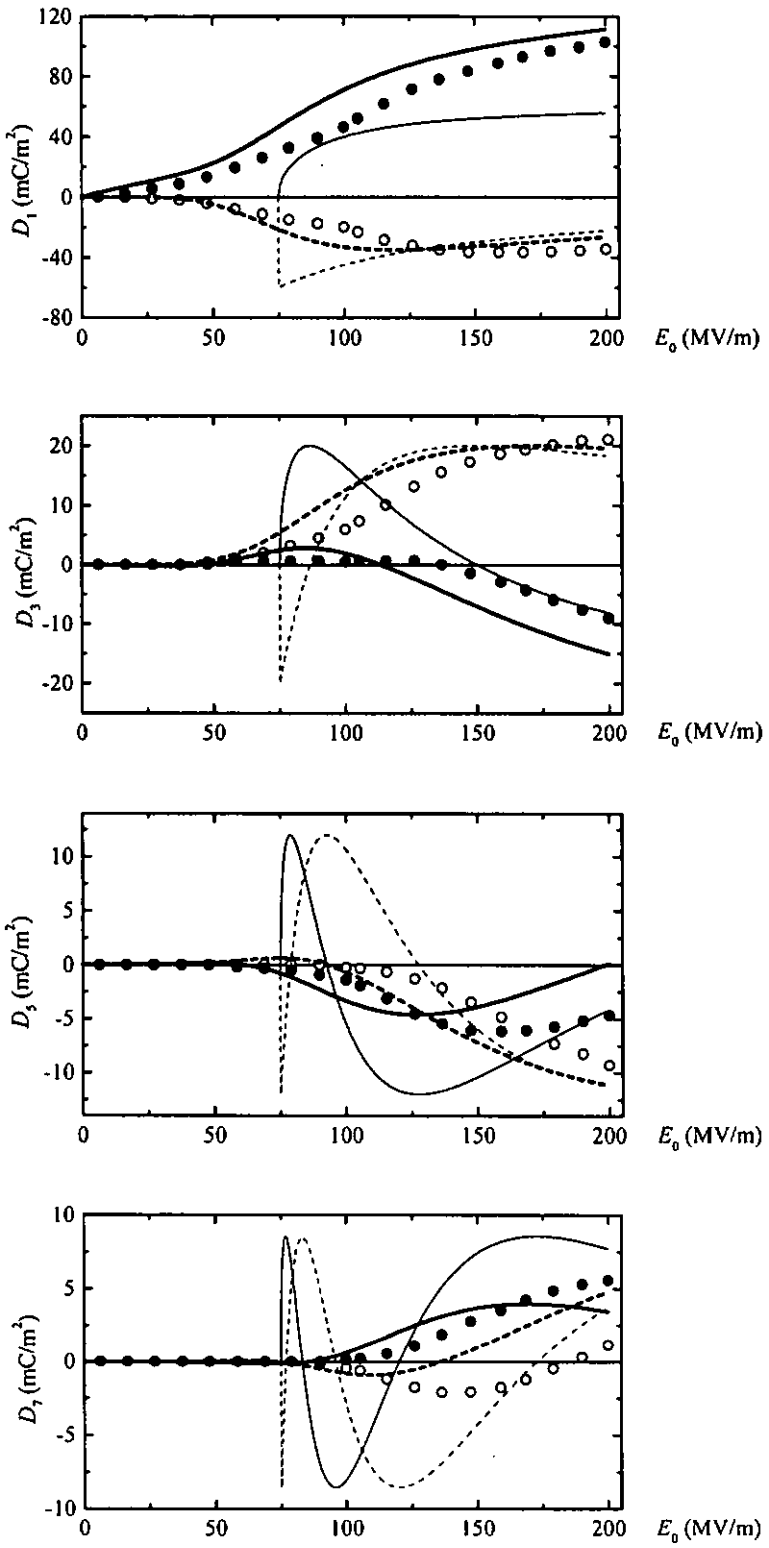

FIG. 3.3 Plot of in-phase, D_n', and out-of-phase, D_n'', components of the 1st, 3rd, 5th and 7th-order of D against E_0 for PVDF. (●) and (○) denote the experimental $D_n'(E_0)$ and $D_n''(E_0)$ respectively. (▬) and (▬ ▬) denote $D_n'(E_0)$ and $D_n''(E_0)$ simulated by using the Preisach model. (——) and (------) denote $D_n'(E_0)$ and $D_n''(E_0)$ calculated from Equations (3.12) and (3.13).

$D_n'(E_0)$ and $D_n''(E_0)$ may then be calculated from the simulated loops, as explained earlier. The $D_n'(E_0)$ and $D_n''(E_0)$ curves are shown in Figure 3.3. For the first-order, third-order and fifth-order components, the broad experimental features are essentially reproduced by the simulations. However, this is not the case with the seventh-order curves. This is because it is quite impossible to find an accurate analytic Preisach function which can reproduce all the fine structures of the experimental curves. From Figure 3.3, it is seen that the experimental curve for the first-order in-phase ions were in good agreement with experimental results. The D-E histories of the copolymer and the electrode material during poling were also obtained.

A Preisach model. In Figure 3.3, by comparing our simulation results with results calculated from the original model used in Furukawa *et al.* [Furukawa *et al.*, 1987], it is seen that the Preisach model gives reasonable $D_n'(E_0)$ and $D_n''(E_0)$ curves with $E_0 < E_c$ (75 MV/m), but the original model cannot. The sudden changes in the original model are missing in the Preisach model. Sudden changes in the calculated $D_n'(E_0)$ and $D_n''(E_0)$ are avoided because of the gradual growth of hysteresis loops. Also, the curves based on the Preisach model are able to account for finer features than the original model.

TABLE 3.2 The parameters of the distributions of α, β, k_0 and k_1 at reference temperature $\theta = 20°C$ used in the Preisach-Landau model.

$\bar{\alpha}$ (10^{11} Vm/C)	σ_α (10^{11} Vm/C)	$\bar{\beta}$ (10^{21} Vm^5/C^3)	σ_β (10^{21} Vm^5/C^3)	σ_{k_0} (M V/m)	σ_{k_1} (M V/m)
235	35	530	200	20	15

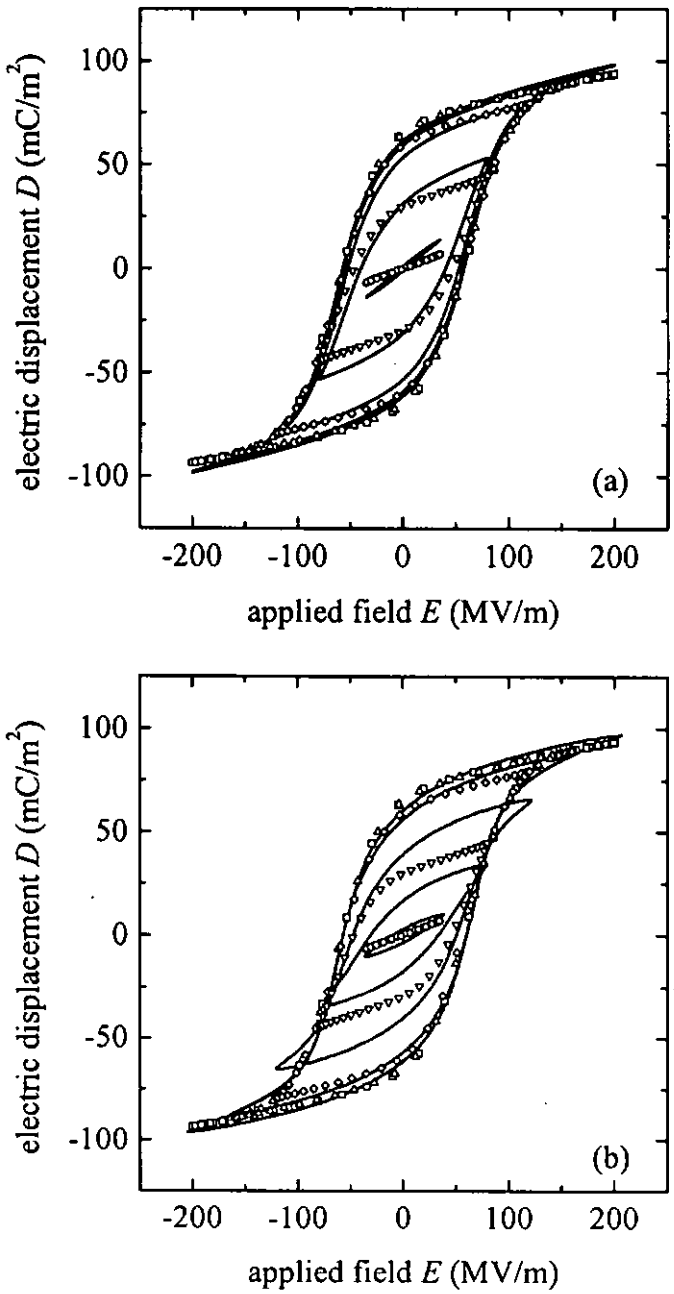

FIG. 3.4 *D-E* loops of PVDF at 20 °C. (a) The Preisach-Landau simulation results (open symbols) are compared with the results obtained from the Preisach model (solid lines). (b) The same simulation results (open symbols) are compared with experimental results in Furukawa *et al.* [Furukawa *et al.*, 1987] (solid lines).

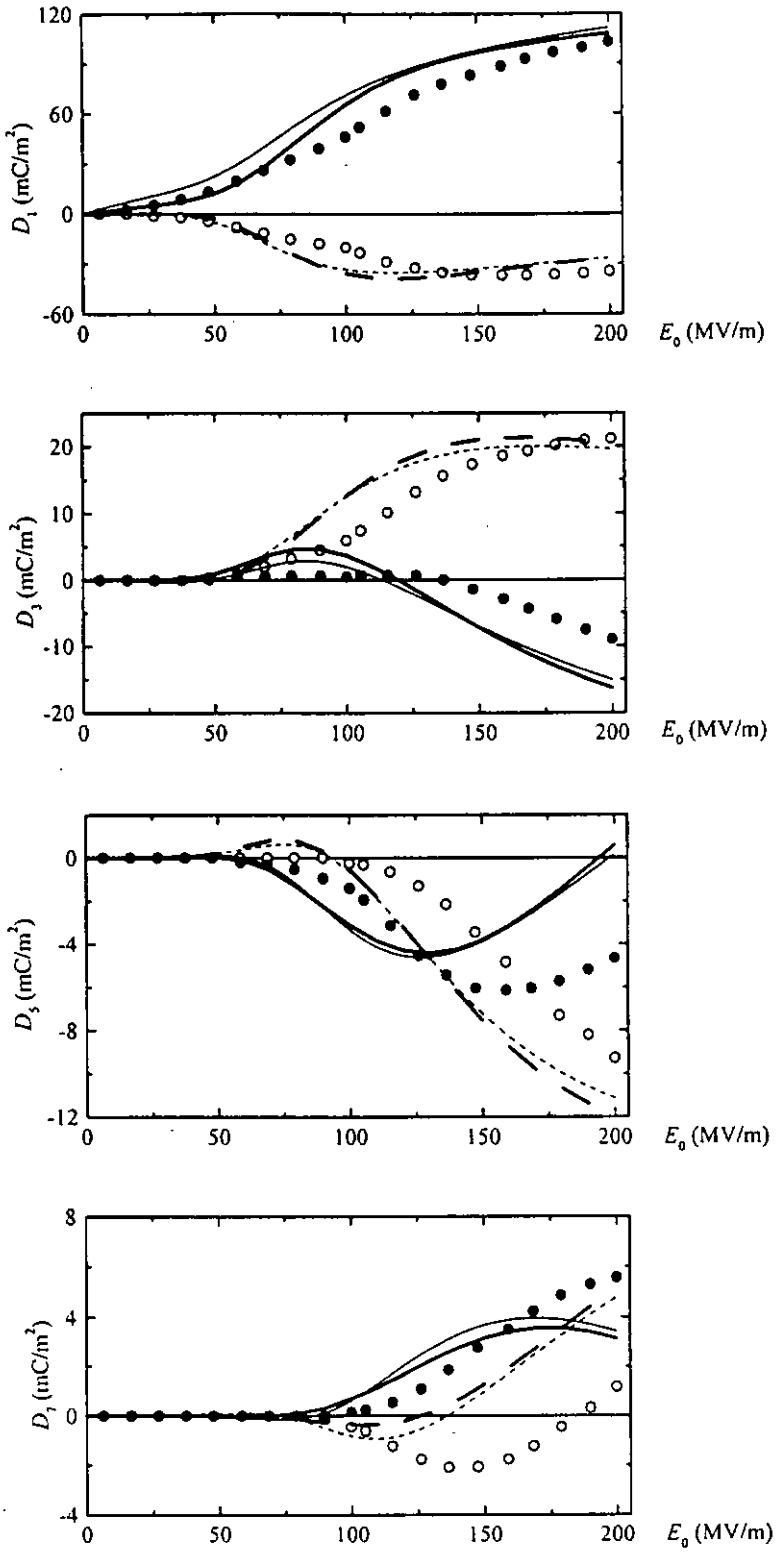

FIG. 3.5 Plot of in-phase, D_n', and out-of-phase, D_n'', components of the 1st, 3rd, 5th and 7th-order of D against E_0 for PVDF. (●) and (o) denote the experimental $D_n'(E_0)$ and $D_n''(E_0)$ respectively. (——) and (– –) denote $D_n'(E_0)$ and $D_n''(E_0)$ simulated by using the Preisach-Landau model. (——) and (------) denote $D_n'(E_0)$ and $D_n''(E_0)$ simulated by using the Preisach model.

Also, a Preisach-Landau model is used for the simulation of nonlinear dielectricity of PVDF. The parameters of the distribution of Landau hysterons for PVDF fitted from the steady-state major hysteresis loop [Furukawa *et al.*, 1987] is shown in Table 3.2. Using these parameters, the *D-E* curves and the curves of the Fourier coefficients, i.e. $D_n'(E_0)$ and $D_n''(E_0)$ curves, for PVDF are calculated and compared with the results from the moving Preisach model.

From Figure 3.4(a) we see that for large E_0 the simulated *D-E* loops are close to the loops obtained from the Preisach model. For small E_0, the difference between the loops produced by the two models becomes obvious. In Figure 3.4(b), the simulated $D(E_0)$ minor loops are larger than the experimental $D(E_0)$ for large E_0, again because every minor loop must lie inside the major loop in a Preisach-Landau model.

For the first-order, third-order and fifth-order components of the $D_n'(E_0)$ and $D_n''(E_0)$ curves (Figure 3.5), both of the simulation results are very close to each other with slightly larger discrepancies in the seventh-order curves. Comparing the Preisach-Landau simulation with the experimental results (Figure 3.5), again almost all key features of the experimental $D_n'(E_0)$ and $D_n''(E_0)$ curves are captured in very much the same manner as the Preisach model can. In comparison with the latter, the Preisach-Landau model is superior with regard to the all-important D_1' and D_1'' coefficients (linear permittivity), which fits the measured data very well up to 70 MV/m, near E_c.

However, in the case of the seventh order curves, noted discrepancy between the simulation and the experimental data occurs. One reason is that the hysteresis loop (or more accurately the μ-E relation) of Landau hysterons in our model is only described up to third powers of μ as $E = -\alpha\mu + \beta\mu^3$, neglecting terms of higher order components (i.e. Equation (2.2)). This affects predictions of the fifth and higher orders of the $D_n'(E_0)$ and $D_n''(E_0)$.

Chapter 4

Study of poling of ferroelectric composites based on Preisach models

4.1 Introduction

In most virgin ferroelectric materials, the piezoelectric and pyroelectric effects are not appreciable so that they cannot be directly used in many applications. A common remedy is to polarize (or to "pole") the materials as highly as possible to magnify the effects and is called poling. Most ferroelectric ceramic materials are brittle and possess cracks, and many exhibit brittle fracture. On the other hand, polymers have high flexibility. Good synergy of ferroelectric ceramic and polymer is achieved by combining the two to form composites. Then, there is the question of how the properties of ferroelectric composites may be predicted accurately. This chapter is a report of an attempt to use the Preisach model and the Preisach-Landau model to study the behavior of multi-layered and 0-3 composites respectively.

4.2 Multi-layered composite system

We analyze the *D-E* response of a multi-layered ferroelectric composite by using

the concepts of the Preisach model to describe each constituent material. Under the assumption that the free charge on each interface is constant, the theory for multi-layered ferroelectric composites is analyzed. The results obtained are compared to *D-E* measurements made in the poling of polyvinylidenefluoride-trifluoroethylene (P(VDF-TrFE)) with ferroelectric triglycine sulfate (TGS) crystal electrodes [Ploss and Ploss, 1996].

4.2.1 Theory

In this work, the electric displacement $D(E)$ of a ferroelectric is written as $P+\varepsilon E$, where P, ε, E are switchable polarization, permittivity and field respectively. Clearly, ε may be determined from the slope of the *D-E* relation in the "saturation" region where $P = P_s$ (see Figure 3.1). Consider a multi-layered composite with n ferroelectric layers, as shown in Figure 4.1. Each constituent material is representable by the Preisach model. Let the field in the i-th constituent material of thickness d_i be E_i if an external field E is applied to the composite and assume that the compensating free charge on each interface remains constant during a *D-E* measurement. When E changes by a small amount ΔE, we have

$$\Delta E = \sum_{i=1}^{n} v_i \Delta E_i \qquad \text{where } v_i = d_i \Big/ \sum_{j=1}^{n} d_j \,. \tag{4.1}$$

The boundary condition $\Delta D_i = \Delta D_{i+1}$ for each interface gives

$$\Delta P_i + \varepsilon_i \Delta E_i = \Delta P_{i+1} + \varepsilon_{i+1} \Delta E_{i+1} \tag{4.2}$$

where D_i, P_i and ε_i represent the electric displacement, the polarization and the permittivity of the i-th constituent material respectively. The susceptibility $\chi(E)$ is defined by dP/dE. Then Equation (4.2) may be rewritten as

$$\chi_i(E_i)\Delta E_i + \varepsilon_i \Delta E_i = \chi_{i+1}(E_{i+1})\Delta E_{i+1} + \varepsilon_{i+1} \Delta E_{i+1}. \tag{4.3}$$

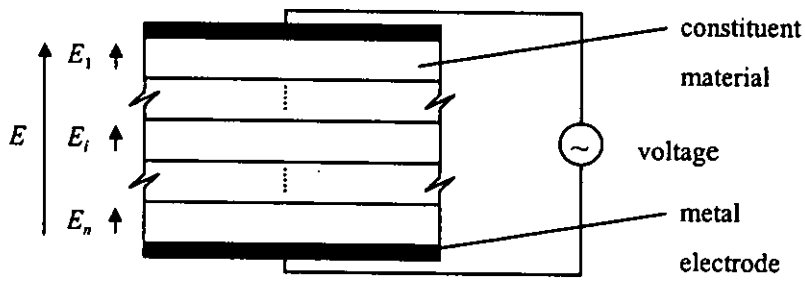

FIG. 4.1 The diagram for multi-layered composite.

Solving Equations (4.1) and (4.3), we can find

$$\Delta E_i = \frac{\prod_{j=1, j\neq i}^{n} \left[\chi_j(E_j) + \varepsilon_j\right] \Delta E}{\sum_{j=1}^{n} \left\{ v_j \prod_{k=1, k\neq j}^{n} \left[\chi_k(E_k) + \varepsilon_k\right] \right\}}. \tag{4.4}$$

Since the change of the electric displacement of the composite ΔD is equal to ΔD_i, so

$$\Delta D = \frac{\sum_{i=1}^{n} \left(v_i \Delta P_i \prod_{j=1, j\neq i}^{n} \varepsilon_j \right) + \prod_{j=1}^{n} \varepsilon_j \Delta E}{\sum_{i=1}^{n} \left(v_i \prod_{j=1, j\neq i}^{n} \varepsilon_j \right)}. \tag{4.5}$$

Noting that the effective properties of the composite are defined by $\Delta D = \Delta P + \varepsilon \Delta E$,

where P and ε represent the polarization and the permittivity of the composite respectively, we have from Equation (4.5)

$$\frac{1}{\varepsilon} = \sum_{i=1}^{n} \frac{v_i}{\varepsilon_i} \tag{4.6}$$

and $$\Delta P = \varepsilon \sum_{i=1}^{n} \frac{v_i}{\varepsilon_i} \Delta P_i = \varepsilon \sum_{i=1}^{n} \frac{v_i}{\varepsilon_i} \left[P_i(E_i + \Delta E_i) - P_i(E_i) \right]. \tag{4.7}$$

Hence, using Equations (1.3), (4.4) and (4.7), ΔD can be calculated if E is changed by ΔE. Thus, the D-E curve can be calculated for a given field history. In this work, the Preisach function is assumed to be given by a Gaussian-Gaussian distribution [Della Torre, 1999]:

$$\mathcal{P}(E_{crit}, E_{int}) = \frac{P_s}{\sqrt{2\pi}\sigma_{crit}} \exp\left[-\frac{(E_{crit} - E_{c0})^2}{2\sigma_{crit}^{\ 2}} \right] \times \frac{1}{\sqrt{2\pi}\sigma_{int}} \exp\left[-\frac{E_{int}^{\ 2}}{2\sigma_{int}^{\ 2}} \right] \tag{4.8}$$

where σ_{crit} is the standard deviation in the critical field, σ_{int} the standard deviation in the interaction field and E_{c0} the average critical field of the Preisach hysterons.

4.2.2 Application to the poling of P(VDF-TrFE) with ferroelectric electrodes

In the article of Ploss and Ploss [Ploss and Ploss, 1996], a ferroelectric electrode poling procedure for P(VDF-TrFE) copolymer of composition 70/30 mol-% by TGS is developed. In this poling technique (Figure 4.2), the initial conditions for the TGS-P(VDF-TrFE)-TGS composite sandwich are $E_{electrode} = E_{copolymer} = 0$ and $D_{electrode}(0) = -P_{rel}$ and $D_{copolymer}(0) = 0$, where P_{rel} is the remanent polarization of the previously poled TGS electrodes. Using Equations (4.4) and (4.7), the D-E curves of the

TGS-P(VDF-TrFE)-TGS stack during poling (Figure 4.2) and of the electrode stack in a subsequent measurement (Figure 4.3) can be simulated.

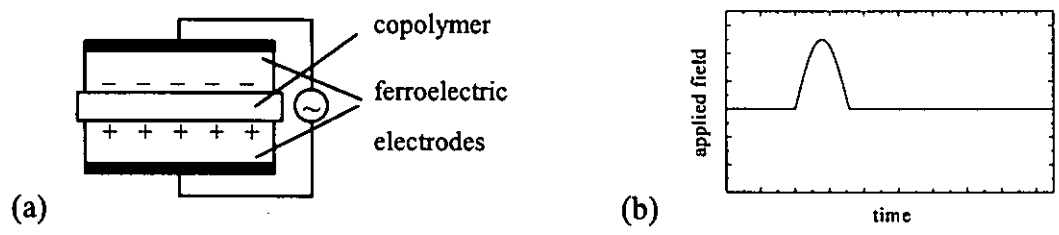

FIG. 4.2 The two identical ferroelectric TGS electrodes are first poled to $-P_{r,el}$, and are separated. In this process, compensating charge is developed on the interfaces. Then, the unpoled copolymer is inserted between the electrodes, shown in (a), to form a triple-layered composite. The composite is poled by applying an external field, shown in (b).

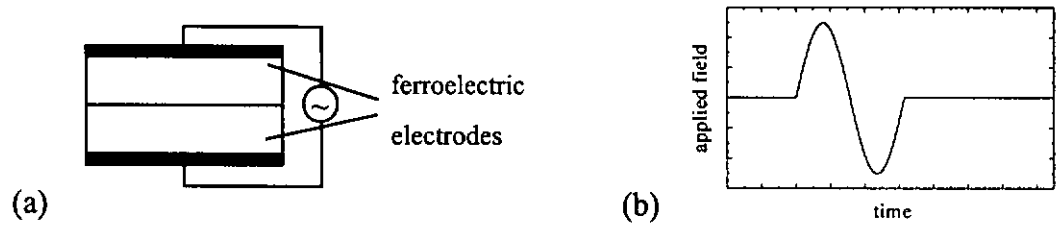

FIG. 4.3 After the poling, the copolymer is removed and the ferroelectric electrodes are stacked together, as shown in (a). A field, shown in (b), is applied to the stack.

4.2.3 Comparison of simulation with experiment

Table 4.1 shows the Preisach parameters and permittivity ε for TGS and P(VDF-TrFE) calculated from the steady-state major hysteresis loops and reversal curves. Using these parameters, the simulated *D-E* curve for the poling of P(VDF-TrFE) with TGS electrodes, i.e. the *D-E* curve of TGS-P(VDF-TrFE)-TGS, is compared with the

experimental result [Ploss and Ploss, 1996], shown in Figure 4.4(a). The *D-E* curve of the electrode stack, i.e. TGS-TGS, after removing the copolymer, is also simulated with result shown in Figure 4.4(b). Essentially, all the broad experimental features are reproduced by the simulations. From Figure 4.4(a), it is seen that the experimental curve is slightly wider than the simulated curve. This discrepancy is most likely due to the experimental fact [Furukawa *et al.*, 1983] that a virgin copolymer sample when first ramped by an electric field can support a slightly higher field before noticeable switching is observed, i.e. higher than the coercive field determined from the steady-state hysteresis loop.

The *D-E* behavior calculated for each constituent material in the poling process is shown in Figure 4.5. The change of D in TGS-P(VDF-TrFE)-TGS is limited by the change of D in TGS. In Figure 4.4(a), the Greek alphabets represent some reference points on the calculated *D-E* curve of TGS-P(VDF-TrFE)-TGS during poling. The corresponding points in the two constituent materials are also shown in Figure 4.5. At λ, the D of the three materials are at turning points because the sign of ΔE_i and ΔE are the same (see Equation (4.4)). At ζ, the field applied to TGS-P(VDF-TrFE)-TGS is zero; however, the field in TGS is negative and that in the copolymer is positive.

In brief, all the broad experimental features are reproduced by the simulations. The *D-E* histories of the copolymer and the electrode material during poling are also obtained.

It is seen that the change of displacement in TGS is limiting the change of the displacement of TGS-P(VDF-TrFE)-TGS.

TABLE 4.1 The Preisach parameters, permittivity and thickness of TGS and P(VDF-TrFE) used in the simulation.

	σ_{crit} (V/μm)	σ_{int} (V/μm)	E_{c0} (V/μm)	P_s (μC/cm^2)	ε (10^{-8}F/m)	d_l (μm)
TGS	0.024	0.03023	0.212	2.865	0.036	1000 [a]
P(VDF-TrFE)	6.2	4.8959	43.48	5.72	0.0109	7 [a]

[a] from Ploss, Bernd and Ploss, Beatrix "Poling of P(VDF-TrFE) with Ferroelectrically Applied Dielectric Displacement". *Ferroelectrics*, Vol. 184, pp. 107-116 (1996)

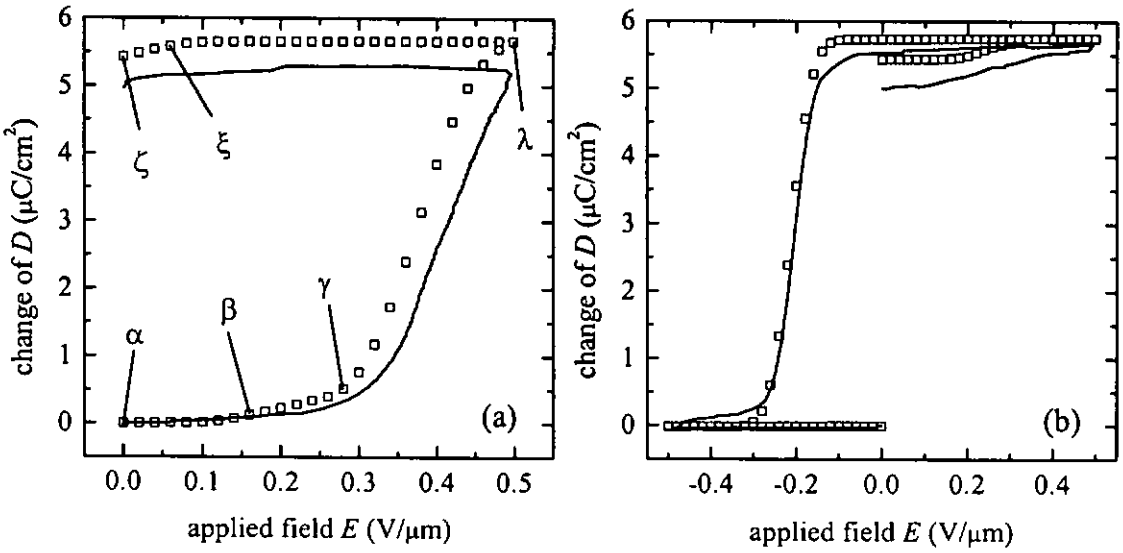

FIG. 4.4 The simulation results (squares) are compared with experimental results [Ploss and Ploss, 1996] (solid line). (a) Change of D in the TGS-P(VDF-TrFE)-TGS composite during poling under conditions shown in Figure 4.2. (b) Change of D in the TGS-TGS stack after removing the copolymer, i.e., under conditions shown in Figure 4.3.

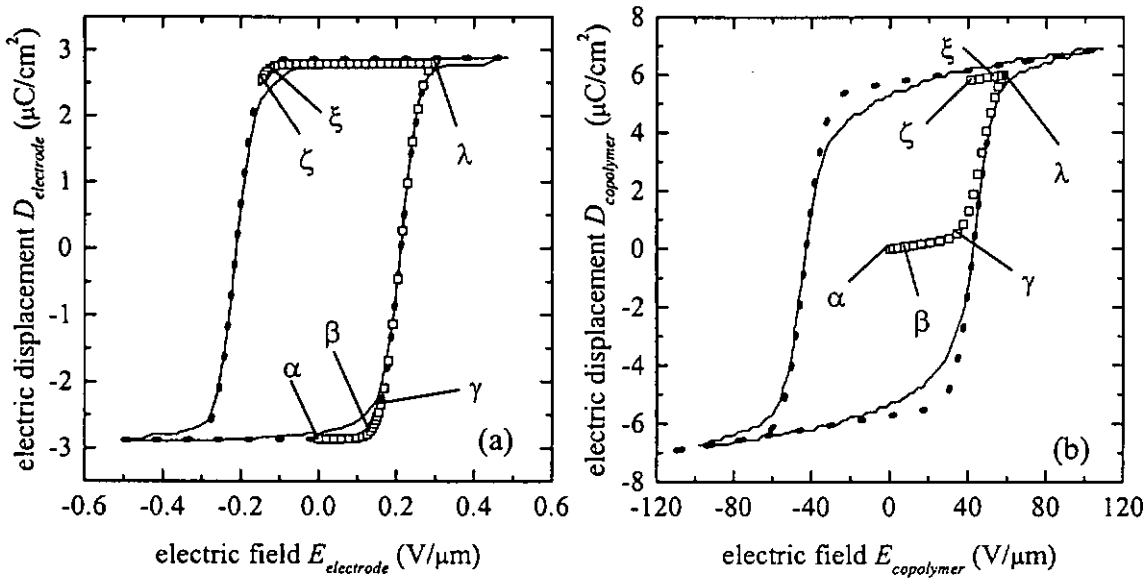

FIG.. 4.5 The squares denote the simulated *D-E* history in a constituent material during poling of TGS-P(VDF-TrFE)-TGS. Corresponding points in the two materials are labeled by Greek alphabets; they are in unison with points in Figure 4.4(a). The dotted and solid lines denote the simulated and experimental major loops respectively of the constituent material. (a) TGS, (b) P(VDF-TrFE).

4.3 0-3 composite system

We consider a composite comprising spherical ferroelectric inclusions in a linear dielectric matrix. The ferroelectric composite is analyzed by using the concepts of a Preisach-Landau model to describe the ceramic inclusions. In the previous section, the modeling study of the multi-layered composite is based on the assumption that the free charge on each interface remains constant. In this section, the charge is allowed to evolve with time. The modeling is used to study several questions of the D.C. poling of 0-3 composite. These include the effects of the poling field magnitude, the poling temperature and the conductivity of the matrix. In this work, we can conclude that the

remanent polarization of the composite can be raised by increasing the poling field or, for the same poling field, by increasing the conductivity of the matrix.

4.3.1 Theory

Again, the electric displacement of a ferroelectric $D(E)$ is written as $P+\varepsilon E$, where P, ε, E are switchable polarization, permittivity and field respectively (see Figure 3.1). Consider a ferroelectric composite comprising a dilute suspension of spherical ferroelectric inclusions, of a material representable by a Preisach-Landau model, in a linear dielectric matrix with permittivity ε_m, under a uniform electric applied field along the polarization direction. The derivative of the average electric field E in the composite can be written as

$$\frac{dE}{dt} = \phi \frac{dE_i}{dt} + (1-\phi)\frac{dE_m}{dt} \tag{4.9}$$

where the subscripts i and m denote "inclusion" and "matrix" respectively and ϕ is the volume fraction of the inclusion phase. The average electric displacement D in the composite is

$$D = \phi D_i + (1-\phi) D_m \tag{4.10}$$

The boundary condition for the inclusion-matrix interface is given by [Wong *et al.*, 2002]

$$D_i + 2\varepsilon_m (E_i - E_m) = D_m + Q \tag{4.11}$$

where Q is the surface charge density on the interface at the pole along the polarization

direction. Since the compensating charge Q is allowed to evolve with time, the electrical conductivities of the materials need to be taken into account. The conduction current densities j in the constituents are

$$j_i = \sigma_i E_i \qquad \text{and} \qquad j_m = \sigma_m E_m \tag{4.12}$$

where σ_i and σ_m are electric conductivities of the inclusion and matrix materials respectively. Since the equations governing the conductivity problem are similar to those used in the dielectrics problem, we have a relation between conduction current densities and electric fields in the constituents similar to Equation (4.11) [Wong *et al.*, 2002]:

$$j_i + 2\sigma_m (E_i - E_m) = j_m - \frac{dQ}{dt}. \tag{4.13}$$

Then, Equation (4.11) can be rewritten as

$$\frac{dD_i}{dE_i}\frac{dE_i}{dt} + 2\varepsilon_m\left(\frac{dE_i}{dt} - \frac{dE_m}{dt}\right) = \varepsilon_m \frac{dE_m}{dt} + \frac{dQ}{dt}. \tag{4.14}$$

Note that ε_m is a constant because the matrix is a linear dielectric material. By solving Equations (4.9) and (4.14), we have

$$\frac{dE_i}{dt} = \frac{3\varepsilon_m \dfrac{dE}{dt} + (1-\phi)\dfrac{dQ}{dt}}{(2+\phi)\varepsilon_m + (1-\phi)\dfrac{dD_i}{dE_i}} \tag{4.15}$$

and $$\frac{dE_m}{dt} = \frac{\left(2\varepsilon_m + \dfrac{dD_i}{dE_i}\right)\dfrac{dE}{dt} - \phi\dfrac{dQ}{dt}}{(2+\phi)\varepsilon_m + (1-\phi)\dfrac{dD_i}{dE_i}}. \tag{4.16}$$

When t changes by a small amount Δt, ΔE_i, ΔE_m and ΔQ can be calculated by using Equations (4.12) and (4.14)-(4.16). Then, ΔD_i and ΔD_m can be found. Using

Equation (4.10), the ΔD-E curve can be calculated for a given field history.

4.3.2 Application to the D.C. poling of 0-3 composite

In this study of poling, a D.C. electric field E_p is applied to a virgin composite, which comprises spherical ferroelectric inclusions in a linear dielectric matrix with $\phi = 0.1$. The field E_p is applied for a sufficiently long time until a steady state is reached, after which the field is released. Under this poling process, we consider different conditions to discuss the variation of the electric displacement of the composite and its constituents. These include (i) the effect of the poling field E_p (Figures 4.7 and 4.8), (ii) the effect of the poling temperature T_p (Figures 4.9 and 4.10) and (iii) the effect of the conductivity σ_m (Figures 4.11 and 4.12). TGS is chosen as an example of the inclusion material in the composite because we already have a Preisach-Landau model for TGS from a previous chapter. We take the Curie temperature T_c as $49.8\,°\mathrm{C}$, and the distributions of α, β, k_0 and k_1 (at reference temperature $\theta = 30\,°\mathrm{C}$) are assumed to be given by Equations (2.27), (2.28), (2.36) and (2.37) respectively. The parameters of these distributions are shown in Table 4.2. The electrical conductivity σ_m and permittivity ε_m of the matrix are 10^{-10} 1/Ωm (at room temperature, σ_m is usually less than σ_i for ceramic/polymer composites [Chan *et al.*, 1995]) and 3.7×10^{-11} F/m (this is a typical value of polymeric materials, such as PVC and epoxy) respectively.

Figure 4.6 shows the major loop of the inclusion material of the 0-3 composite with the parameters of the distribution of Landau hysterons, given in Table 4.2. It is seen that the coercive field E_{ci} of the material is 71680 V/cm, which is two orders of magnitudes larger than the experimental value (410 V/cm [Triebwasser, 1958]). Indeed, many experiments indicate that the experimental values are several orders of magnitude lower than the values calculated from the Landau theory [Jona and Shirane, 1962; Kim *et al.*, 2002]. This discrepancy is due to the mechanism of motion of domain walls in polarization growth rather than dipole switching. To enable a Preisach-Landau model to study real situations such as the poling of composites, we (at least tentatively) describe the hysteresis loop of a Landau hysteron by "reduced" parameters, the net effect of which is to scale the calculated E fields to realistic values, that is,

$$\frac{E(\text{real})}{E_c(\text{real})} = \frac{E(\text{calculated})}{E_c(\text{calculated})}. \tag{4.17}$$

The advantage is that the formulation of the model does not become more difficult but can describe "real" hysteresis loops of materials, which is what is needed here.

TABLE 4.2 The Curie temperature T_c and electrical conductivity σ_i and parameters of the distributions of α, β, k_0 and k_1 for TGS at $\theta = 30$ °C used in the simulation.

$\bar{\alpha}$ (10^6 Vm/C)	σ_α (10^6 Vm/C)	$\bar{\beta}$ (10^{10} Vm^5/C^3)	σ_β (10^{10} Vm^5/C^3)
685.7	41.05	99.64	70
σ_{k_0} (10 V/cm)	σ_{k_1} (10 V/cm)	σ_i (1/Ωm)	T_c (°C)
50	821.1	10^{-9}	49.8

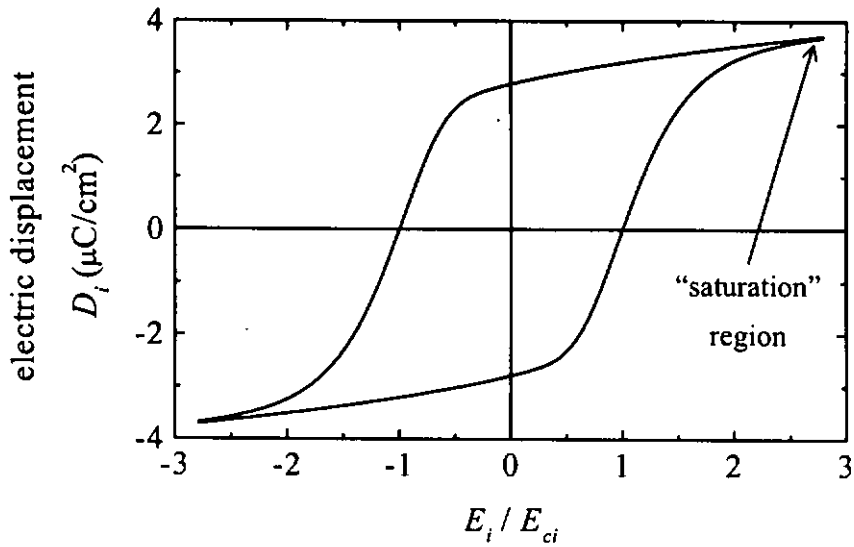

FIG. 4.6 The major loop of the ferroelectric inclusion in the 0-3 composite at 30 °C.

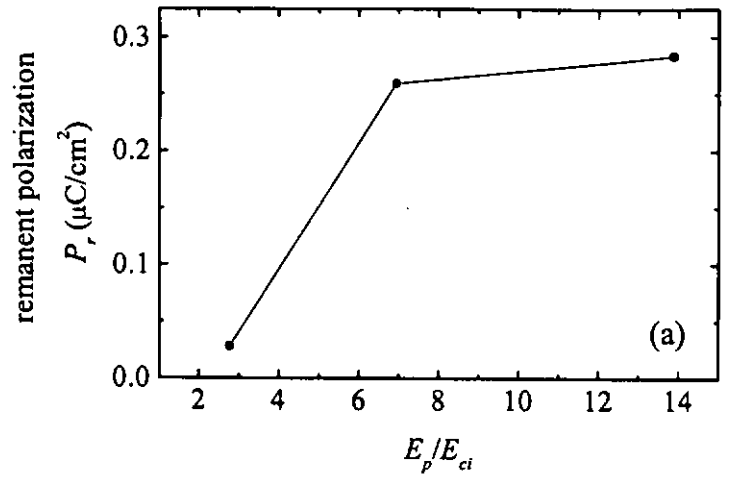
remanent polarization
P_r (μC/cm²)
0.0
0.1
0.2
0.3
2
4
6
8
10
12
14
E_p/E_{ci}
(a)

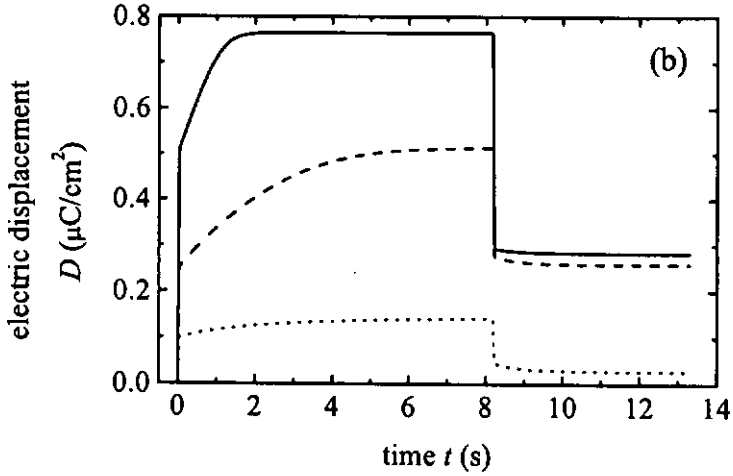
electric displacement
D (μC/cm²)
0.0
0.2
0.4
0.6
0.8
0
2
4
6
8
10
12
14
time t (s)
(b)

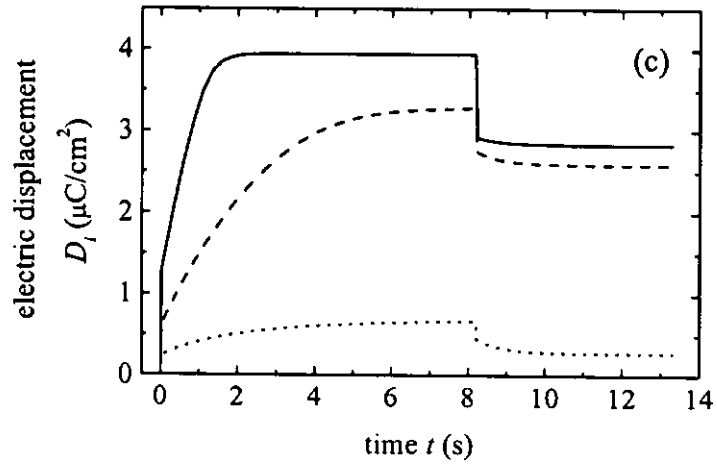
electric displacement
D_l (μC/cm²)
0
1
2
3
4
0
2
4
6
8
10
12
14
time t (s)
(c)

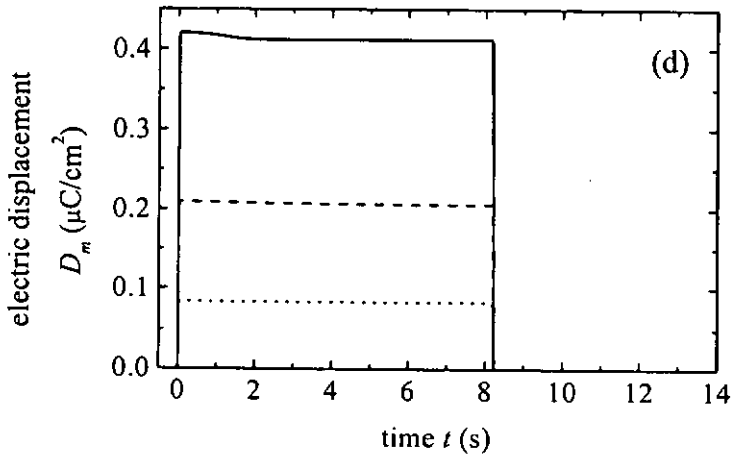
electric displacement
D_m (μC/cm²)
0.0
0.1
0.2
0.3
0.4
0
2
4
6
8
10
12
14
time t (s)
(d)

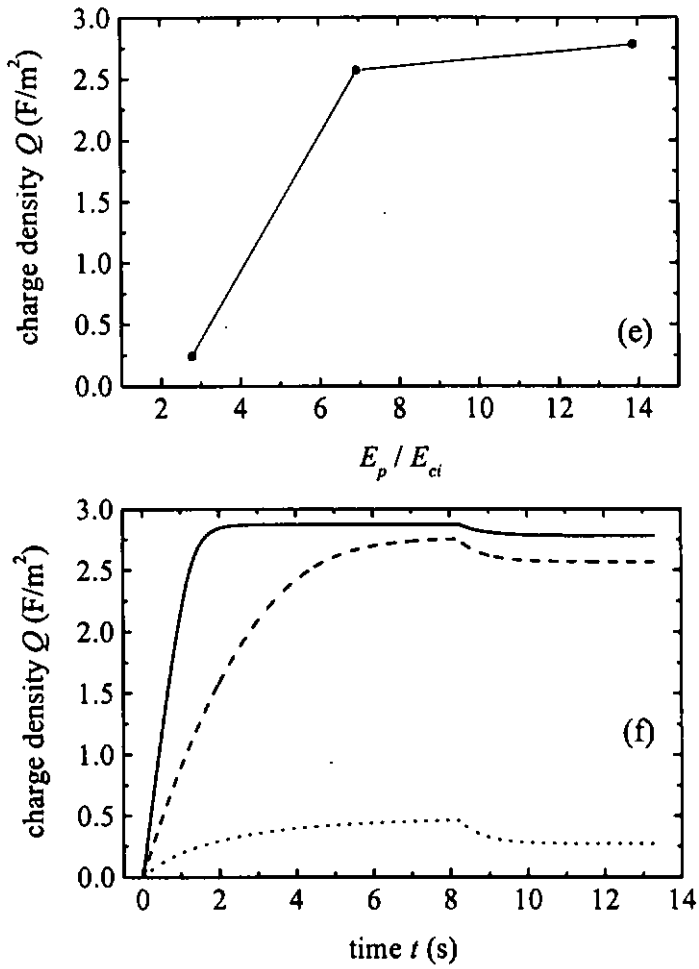

FIG. 4.7 (a) The variation of the remanent polarization P_r of the composite after poling with poling field E_p. (—), (---) and (.....) denote $E_p = 14E_{ci}$, $E_p = 7E_{ci}$ and $E_p = 2.8E_{ci}$ respectively. The corresponding time variation of the electric displacement of (b) the composite, (c) the inclusion and (d) the matrix under different E_p. (e) The variation of the interfacial charge density Q after poling with poling field E_p. (f) The corresponding time variation of the interfacial charge density Q.

4.3.2.1 Effect of poling field

After poling, a steady state for the composite is reached with sufficiently long time. Figure 4.7(a) shows the variation of the remanent polarization P_r of the composite after poling with poling field E_p. The remanent polarization P_r increases as E_p increases; and their relationship is nonlinear. Also, it is seen that when E_p is large enough, the increment of P_r becomes small. This is because the poling process induces the saturation behavior of the ferroelectric inclusion material. The increment of the electric displacement D_i of the inclusion in the "saturation" region is small with respective to an increment of field E_i (see Figures 3.1 and 4.6). From Figure 4.6, the field strength around the saturation region is about $2.65\,E_{ci}$, and the corresponding D_i is 3.6 μC/cm^2. This effect, i.e. saturation behavior of the inclusion, can be observed in Figure 4.7(c).

In Figure 4.7(c), at the steady state region with the poling field on, the inclusion is poled to near saturation as E_p is greater than $7\,E_{ci}$, and the increment in D_i with a larger E_p is small, unlike the case of $E_p < 7E_{ci}$. Simultaneously, in Figure 4.7(b), the increment of D is also small because the matrix is a linear dielectric material which has no saturation behavior (see Figure 7(d)), so that the D of the composite behaves as the D_i of the inclusion.

Noting that the fields in the two constituents must eventually go to zero after the poling field is released, thus D_i, D_m and therefore D drop when the poling field E_p is

released, as shown in Figures 4.7(b), (c) and (d). The sudden drop is due to the dE/dt term in Equations (4.15) and (4.16). After the poling process is finished, P_{ri} is close to the remanent polarization of the inclusion since the inclusion is poled to near saturation under $E_p > 7E_{ci}$. Based on this effect, P_r is also close to ϕP_{ri}, which is the maximum value of the remanent polarization of the composite after poling (see Figure 4.7(b)).

From Figures 4.7(e) and (f), we see that the time variation of the interfacial charge density Q after poling with poling field E_p is nonlinear. Since E_i and E_m would go to zero after poling, by Equation (4.11) Q after poling is equal to D_i (see Figure 4.7(c)). From the above observations of the variation of D_i with E_p, we know that this effect is also due to the saturation behavior of the inclusion.

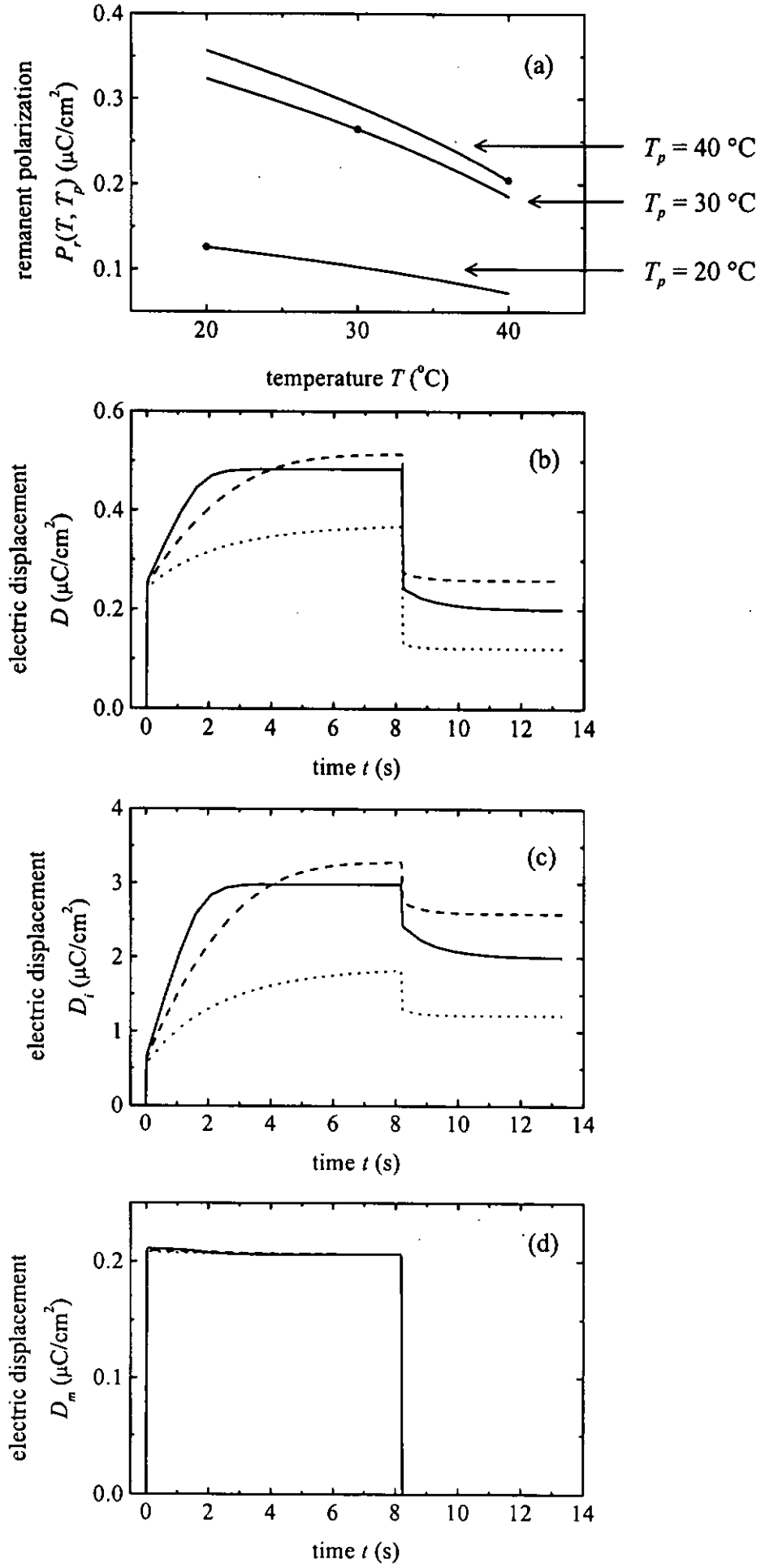
(a)
remanent polarization
$P_r(T, T_p)$ (μC/cm²)
0.4
0.3
0.2
0.1
20
30
40
temperature T (°C)
T_p = 40 °C
T_p = 30 °C
T_p = 20 °C
(b)
electric displacement
D (μC/cm²)
0.6
0.4
0.2
0.0
0
2
4
6
8
10
12
14
time t (s)
(c)
electric displacement
D_i (μC/cm²)
4
3
2
1
0
0
2
4
6
8
10
12
14
time t (s)
(d)
electric displacement
D_m (μC/cm²)
0.2
0.1
0.0
0
2
4
6
8
10
12
14
time t (s)

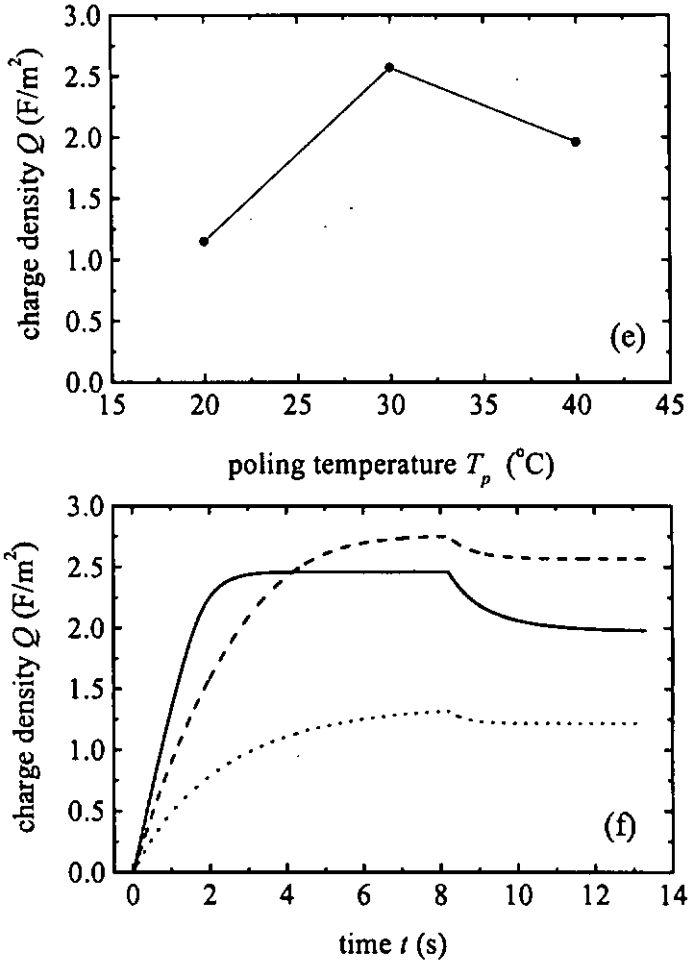

FIG. 4.8 (a) The variation of the remanent polarization P_r of the composite at temperature T after poling with poling temperature T_p. The upper, middle and lower dash dotted lines denote T_p = 40 °C, T_p = 30 °C and T_p = 20 °C respectively. (—), (- - -) and (·····) denote T_p = 40 °C, T_p = 30 °C and T_p = 20 °C. The corresponding time variation of the electric displacement of (b) the composite, (c) the inclusion and (d) the matrix at temperature T_p with poling temperature T_p. (e) The variation of the interfacial charge density Q at temperature T after poling with poling temperature T_p. (f) The corresponding time variation of the interfacial charge density Q.

4.3.2.2 Effect of poling temperature

A D.C. field $E_p = 7E_{ci}$ is applied to the composite at different temperatures T_p. Based on the definitions of α, β and E_{int} (see Sections 2.2.4 and 2.5.1), the parameters of the distributions of α and E_{int} change as T_p changes. In this simulation, the electrical conductivities of the constituent materials of the composite are assumed to be constants since a relatively narrow temperature variation (20-40 °C) is considered here. Let $P_r(T,T_p)$ denote the remanent polarization of the composite at temperature T after poling at temperature T_p. Figure 4.8(a) (solid circles) shows the variation of the remanent polarization $P_r(T_p,T_p)$ of the composite at temperature T_p after poling at temperature T_p and Figure 4.8(b) shows the time variation of the electric displacement of the composite during poling at temperature T_p. We see that, under the same poling field E_p, the relation between $P_r(T_p,T_p)$ and T_p is not monotonic, due to the intrinsic properties of Landau hysterons of the inclusions. The critical field and electric displacement of Landau hysterons decrease as temperature increases (see Figure 2.7). Hence, the poling field E_p for fully polarizing the inclusion at high T_p is smaller than that for low T_p. This can be observed in Figure 4.8(c). At $T_p = 40\,°\mathrm{C}$, the inclusion is polarized to saturation. At $T_p = 30\,°\mathrm{C}$, the inclusion is also near saturation, but the inclusion is unsaturated when poled at $T_p = 20\,°\mathrm{C}$. However, the remanent polarization of the inclusion at high T_p is smaller than that at low T_p (see Figure 2.7). Based on these

two effects, the variation of $P_r(T_p,T_p)$ with poling temperature T_p may not be monotonic.

In the Landau theory for the second order phase transition, the remanent polarization $P_r(T)$ of a material at temperature T is $\sqrt{\alpha_0(T_c-T)/\beta}$ (from Equation (1.18)). We define $\eta(T,T_p)$ as the ratio of $P_r(T)$ to $P_r(T_p)$, i.e.

$$\eta(T,T_p)=\frac{P_r(T)}{P_r(T_p)}=\frac{\sqrt{\alpha_0(T_c-T)/\beta}}{\sqrt{\alpha_0(T_c-T_p)/\beta}}=\sqrt{\frac{T_c-T}{T_c-T_p}} \tag{4.18}$$

which is greater than one if $T<T_p<T_c$. After poling, E_i and E_m would eventually go to zero and therefore the remanent polarization $P_r(T_p,T_p)$ of the composite should only depend on the remanent polarization $P_{ri}(T_p,T_p)$ of the inclusion because the matrix is a linear dielectric.

Now consider bringing the samples polarized at different T_p's to the same temperature T. Assume that the remanent polarization $P_{ri}(T,T_p)$ of the inclusion at temperature T equals $\eta(T,T_p)P_{ri}(T_p,T_p)$ as in the above analysis. (This assumption only provides an approximate $P_{ri}(T,T_p)$). Since $P_r(T_p,T_p)=\phi P_{ri}(T_p,T_p)$ after poling, $P_r(T,T_p)$ is monotonic increasing with T_p, as shown in Figure 4.8(a). This means that the remanent polarization $P_r(T,T_p)$ of the composite becomes higher if T_p is higher.

Figures 4.8(e) and (f) show the variation of the interfacial charge density Q after poling at T_p and the time variation of the interfacial charge density respectively. Similar to the case of the Q in the previous section, Q is equal to $P_{ri}(T_p,T_p)$ after poling.

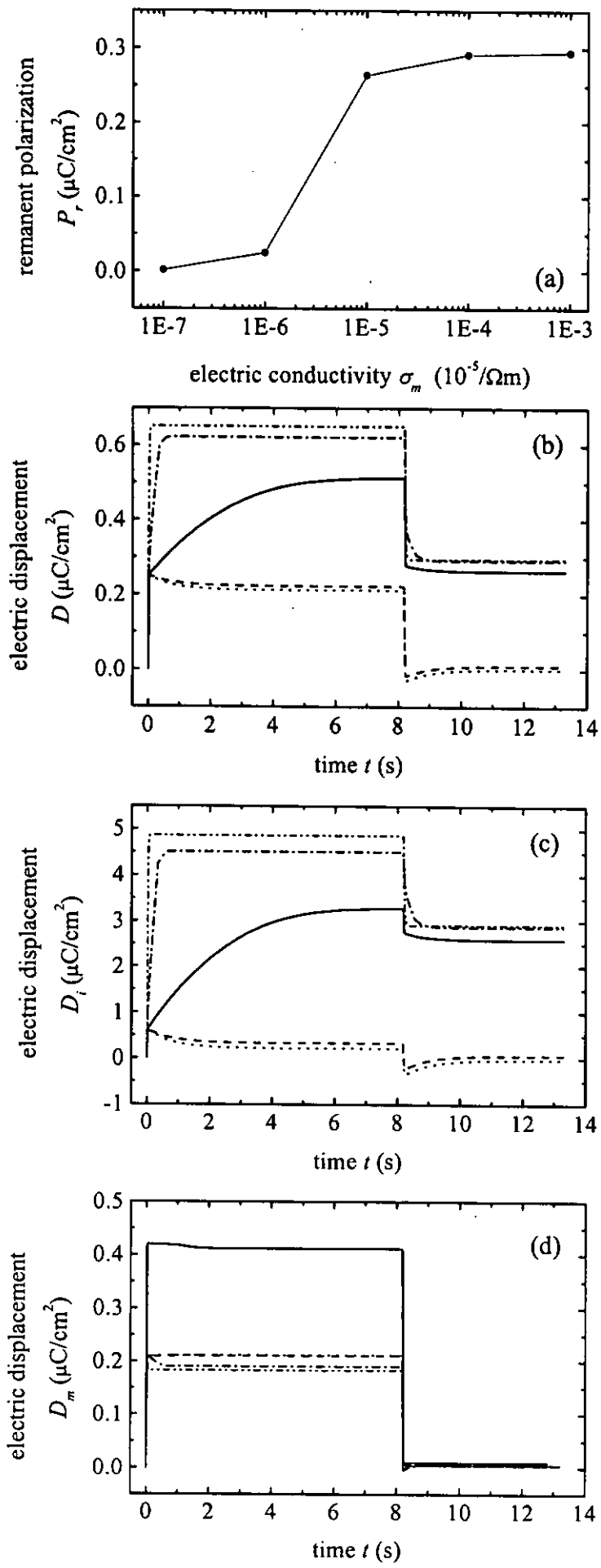
remanent polarization
P_r (μC/cm²)
0.3
0.2
0.1
0.0
(a)
1E-7
1E-6
1E-5
1E-4
1E-3
electric conductivity σ_m (10^{-5}/Ωm)
electric displacement
D (μC/cm²)
0.6
0.4
0.2
0.0
(b)
0
2
4
6
8
10
12
14
time t (s)
electric displacement
D_i (μC/cm²)
5
4
3
2
1
0
-1
(c)
time t (s)
electric displacement
D_m (μC/cm²)
0.5
0.4
0.3
0.2
0.1
0.0
(d)
time t (s)

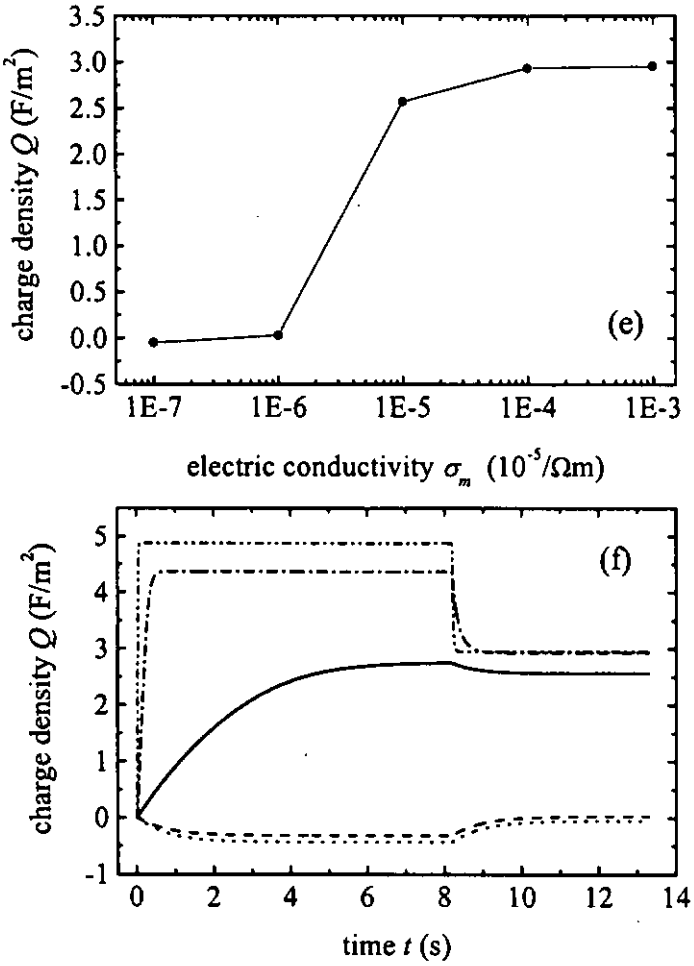

FIG. 4.9 (a) The variation of the remanent polarization P_r of the composite with the electric conductivity of the matrix σ_m. (—··), (-·-), (—), (---) and (·····) denote $\sigma_m = 10^{-8}$ 1/Ωm, $\sigma_m = 10^{-9}$ 1/Ωm, $\sigma_m = 10^{-10}$ 1/Ωm, $\sigma_m = 10^{-11}$ 1/Ωm and $\sigma_m = 10^{-12}$ 1/Ωm respectively. The corresponding time variation of the electric displacement of (b) the composite, (c) the inclusion and (d) the matrix under different σ_m. (e) The variation of the interfacial charge density Q with σ_m.

4.3.2.3 Effect of the conductivity of the matrix in 0-3 composite

A D.C. field $E_p = 7E_{ci}$ is applied to the composite. Figure 4.9(a) shows the variation of the remanent polarization P_r of the composite with the conductivity of the matrix σ_m after poling. The remanent polarization P_r of the composite increases as the conductivity of the matrix σ_m increases. Also, P_r is almost zero if σ_m is too small. The reason is that the field E_m in the matrix decreases when σ_m increases. As a result, the field E_i in the inclusion becomes larger. Therefore, the value of D_i and D can be raised (see Figures 4.9(b) and (c)).

Figure 4.9(e) shows the variation of the interfacial charge density Q with σ_m. We see that the behavior of Q is similar to that of D_i after poling.

Chapter 5

Conclusions

The Preisach model is used for modeling nonlinear behavior in ferroelectrics and ferroelectric composites. In addition, a new model, the "Preisach-Landau" model, of ferroelectric behavior based on a combination of the Preisach model and the Landau theory for the second order phase transition of ferroelectrics is developed. This is the first of such an attempt to replace Preisach hysterons by Landau hysterons. The new model allows discussion on phase transition and the effect of temperature on physical properties, which the Preisach model cannot tackle. Also, minor loops which the Landau theory cannot describe are now produced by the model.

For a fixed temperature below the Curie temperature, a Preisach-Landau model retains the deletion property and the property of equal vertical chords of the classical Preisach model, but not the congruency property. The latter should not be taken as a complaint because many real materials do not exhibit the congruency property. Broad features of the temperature dependence of ferroelectric properties such as coercive field, remanent polarization and dielectric constant are reproduced by this model in agreement with the Landau theory. The Landau model is a special case of this model without the

distribution of hysterons. The power of the present model, or a model combining Preisach's ideas with ferroelectric transitions, lies in its ability to discuss the behavior of a ferroelectric material subjected to arbitrary field history. Notwithstanding a fair amount of success made possible by this approach, the variation of coercive field of TGS material as a function of temperature calculated as an example in this work, although agreeing with the Landau theory, do not describe real TGS material well.

The Preisach-Landau model of Section 2.2 assumes the interaction field $E_{int} = k_{10}(T_c - T)$. Although this can simulate the well-known characteristic V-shaped $1/\varepsilon_r$-T curve of a second order ferroelectric (see Figure 2.9), the dielectric constant has an infinite value at T_c which is not the case in TGS, for instance. In Section 2.5, a more refined Preisach-Landau model is proposed to tackle features such as finite dielectric constant at T_c. Here the interaction field is written as $E_{int} = k_{10}(T_c - T) + k_0$ where k_0 and k_{10} are real numbers with a distribution. This model thus reproduces a finite reciprocal dielectric constant at the transition and a rounded V-shape around the transition temperature. Comparing with the experimental results [Gaffar *et al.*, 1989], this modification is able to account for finer features of the experimental $1/\varepsilon_r$-T curve.

The nonlinear dielectricity of the electric displacement of a ferroelectric is studied. Using the concepts of the Preisach model, the *D-E* loops of different field amplitudes are simulated and Fourier analyzed. Both in-phase and out-of-phase components of the

Fourier coefficients obtained are compared with the experimental data for PVDF [Furukawa *et al.*, 1987]. Essentially, the simulations reproduce almost all the broad experimental features of the lower harmonics. As a finer point, in the region near E_c, this model avoids a sharp change of the Fourier coefficients of D occurring in the model of the original paper.

On the other hand, a Preisach-Landau model is also used for the simulation of nonlinear dielectricity of PVDF. Comparing the Preisach-Landau simulation with the experimental results, almost all key features of the experimental curves are captured in very much the same manner as the Preisach model can. However, in comparison with the latter, the Preisach-Landau model is superior with regard to the all-important D_1' and D_1'' coefficients (linear permittivity), which fits the measured data very well up to near E_c.

In the studies of the poling of ferroelectric composites, a multi-layered ferroelectric composite is first studied by using the classical Preisach model to describe each constituent material. Under the assumption that the free charge on each interface is constant, the theory for multi-layered ferroelectric composites is analyzed. The theory is then applied to study the poling of P(VDF-TrFE) with TGS electrodes [Ploss and Ploss, 1996]. All the essential experimental features are reproduced by the simulations. It is seen that the change of electric displacement in TGS is limiting the change of the

displacement of the TGS-P(VDF-TrFE)-TGS sandwich. The *D-E* histories of the copolymer and the electrode material during poling are also obtained.

For 0-3 composites, we consider the poling of a composite comprising spherical ferroelectric inclusions in a linear dielectric matrix. The ferroelectric composite is analyzed by using a Preisach-Landau model to describe each constituent material. The free charge on the inclusion-matrix interface is allowed to evolve with time. In this work, a D.C. electric field E_p is applied to a virgin composite of TGS/polymer with $\phi = 0.1$ until a steady state is reached, then the field E_p is released. Under this poling process, we consider different conditions to discuss the variation of electric displacement of the composite and its constituents. These include the effect of (i) the poling field E_p, (ii) the poling temperature T_p and (iii) the conductivity of the matrix σ_m.

In the study of the effect of E_p, after poling, the remanent polarization P_r of the composite increases with the poling field E_p. The relation between P_r and E_p is nonlinear because of the saturation behavior of the electric displacement of the inclusion. In the study of the effect of poling temperature T_p, after poling with a fixed poling field E_p, the remanent polarization of the composite at temperature T_p as a function of poling temperature T_p is not monotonic. It is shown that when the poled samples are brought back to the same temperature *T*, then $P_r(T,T_p)$ at temperature *T* is larger as T_p increases. Finally, in the study of the effect of σ_m, a small σ_m implies a small value of *D* after

poling. It is because the field in the matrix increases as σ_m decreases. In brief, the remanent polarization $P_r(T,T_p)$ of the composite can be raised by increasing the poling field, the poling temperature and the matrix conductivity.

In this project, a Preisach-Landau model is applied to study the nonlinear behavior of ferroelectrics. However, the simulated coercive field of ferroelectric is two orders of magnitudes larger than the experimental value since we use Landau hysterons together with the Preisach idea. Due to this discrepancy, the application of the Preisach-Landau model is hampered because it does not describe very well a "real" hysteresis for ferroelectrics. Therefore, further theoretical investigation in avoiding this discrepancy would seem to be essential. In the literature, one approach to give a more realistic free energy for a "Landau" material (in our case, the free energy of Landau hysteron) is to incorporate terms for considering the effect of domain walls and interaction among dipoles in the material [Lines and Glass, 1977; Kim *et al.*, 2002].

On the other hand, many ferroelectric materials undergo a first order ferroelectric-paraelectric phase transition. In our project, the Preisach-Landau model only discusses the case for the second order phase transition. An extension of the model to "first order" materials is valuable. In the studies of the properties of ferroelectrics, such as piezoelectric and pyroelectric properties and the effect of frequency on the hysteresis loop, the use of the Preisach-Landau model would seem attractive and valuable; here a

modification of the Landau hysteron in the model is envisaged. In the literature, several approaches are helpful for this modification. Freeman and Joshi [Freeman and Joshi, 1996] suggested to modify the Preisach hysteron in a ferroelectric to take into account the effect of applied stress. Briefly, the "shape" of the Preisach hysteron changes as stress is applied to the material so that the Preisach model can discuss the variation of the hysteresis loop due to the effect of stress and strain. Further, the Landau-Khalatnikov theory is also suitable to describe the hysteresis loop of Landau hysterons with variation in frequency. Thus the hysterons may better describe the coercive field of a "real" ferroelectric and allow realistic discussion on the effect of frequency on hysteresis loop.

List of publications

Tsang, C.H., Ploss, B., Ploss, B. and Shin, F.G. "Simulation of the poling of P(VDF-TrFE) with ferroelectric electrodes based on the Preisach model". *Ferroelectrics*, Vol. 259, pp. 139-144 (2001)

Tsang, C.H. and Shin, F.G. "Simulation of nonlinear dielectric properties of polyvinylidene fluoride based on the Preisach model". *Journal of Applied Physics*, (to appear in the February 1, 2003 issue)

Tsang, C.H. and Shin, F.G. "A model of ferroelectric behavior based on a combination of the Preisach model and the Landau theory". *Journal of Applied Physics*, (submitted)

Tsang, C.H. and Shin, F.G. "Behavior of dielectric constant near Curie temperature based on a Preisach-Landau model" (manuscript ready)

References

Andrei, P. and Stancu, A. "Identification method analyses for the scalar generalized moving Preisach model using major hysteresis loops". *IEEE Transactions on Magnetics*, Vol. 36, pp. 1982-1989 (2000)

Bartic, A.T., Wouters, D.J., Maes, H.E., Rickes, J.T. and Waser, R.M. "Preisach model for the simulation of ferroelectric capacitors". *Journal of Applied Physics*, Vol. 89, pp. 3420-3425 (2001)

Basso, V. and Bertotti, G. "Description of magnetic interactions and Henkel Plots by the Presiach hysteresis model". *IEEE Transactions on Magnetics*, Vol. 30, pp. 64-72 (1994)

Bate, G. "Statistical stability of the Preisach diagram for particles of γ-Fe_2O_3". *Journal of Applied Physics*, Vol. 33, pp. 2263-2269 (1962)

Bertotti, G. *Hysteresis in Magnetism for Physicists, Materials Scientists, and Engineers*. San Diego: Academic Press (1998)

Chan, H.L.W., Chen, Y. and Choy, C.L. "A poling study of PZT/P(VDF-TrFE) copolymer 0-3 composites". *Ferroelectrics*, Vol. 9, pp. 207-214 (1995)

Chen, W. and Lynch, C.S. "A model for simulating polarization switching and AF-F phase changes in ferroelectrics ceramics". *Journal of Intelligent Material Systems and Structures*, Vol. 9, pp. 427-431 (1998)

Chincholkar, V.S. and Unruh, H.G. "Surface layers of triglycine sulfate single crystals".

Physica Status Solidi A, Vol. 29, pp. 669-673 (1968)

Cornejo, D.R., Bue, L.M., Basso, V., Bertotti, G. and Missell, F.P. "Moving Presiach model analysis of nanocrystalline SmFeCo". *Journal of Applied Physics*, Vol. 81, pp. 5588-5590 (1997)

Craig, P.P. "Critical phenomena in ferroelectrics". *Physics Letters*, Vol. 20, pp. 140-142 (1966)

Deguchi, K. and Nakamura, E. "Critical region in ferroelectric triglycine sulfate". *Physical Review B*, Vol. 5, pp. 1072-1073 (1972)

Della Torre, E. "A Preisach model for accommodation". *IEEE Transactions on Magnetics*, Vol.30, pp. 2701-2707 (1994)

Della Torre, E. and Vajda, F. "Parameter identification of the complete-moving-hysteresis model using major loop data". *IEEE Transactions on Magnetics*, Vol. 30, pp. 4987-5000 (1994)

Della Torre, E. *Magnetic Hysteresis*. New York: IEEE Press (1999)

Ehses, K.H. and Schmitt, H. "The temperature dependence of the spontaneous polarization of TGS near the phase transition". *Ferroelectrics*, Vol. 21, pp. 543-544 (1978)

Freeman, A.R. and Joshi, S.P. "Numerical modeling of PZT nonlinear electromechanical behavior". In Varadan, V.V., ed., *Proceedings of the SPIE - The International Society for Optical Engineering*, Vol. 2715, San Diego, 26-29 February, 1996, pp. 602-613 (1996)

Furukawa, T., Lovinger, A.J., Davis, G.T. and Broadhurst, M.G. "Dielectric hysteresis and nonlinearity in a 52/48 mol percent co-polymer of vinylindene fluoride and trifluoroethylene". *Macromolecules*, Vol. 16, pp. 1885-1890 (1983).

Furukawa, T., Nakajima, K., Koizumi, T. and Date, M. "Measurements of Nonlinear Dielectricity in Ferroelectric Polymers". *Japanese Journal of Applied Physics*, Part 1 Vol. 26, pp. 1039-1045 (1987)

Gaffar, M.A., Al-Noaimi, G.F. and Abu El-Fadl, A. "Critical behaviour of dielectric permittivity and spontaneous polarization of triglycine sulphate single crystals doped with organic molecules". *Journal of the Physical Society of Japan*, Vol. 58, pp. 3392-3400 (1989)

Gonzalo, J.A. "Equation of state for the cooperative transition of triglycine sulfate near T_c". *Physical Review B*, Vol. 7, pp. 3125-3132 (1970)

Hall, D.A. "Nonlinearity in piezoelectric ceramics". *Journal of Materials Science*, Vol. 36, pp. 4575-4601 (2001)

Hughes, D. and Wen, J.T. "Preisach modeling of piezoceramic and shape memory alloy hysteresis". *Smart Material Structures*, Vol. 6, pp. 287-300 (1997)

Huo, Y. "A mathematical model for the hysteresis in shape memory alloys". *Continuous Mechanism Thermodynamics*, Vol. 1, pp. 283-303 (1989)

Jona, F. and Shirane, G. *Ferroelectric Crystals*, Oxford: Pergamon Press, pp. 21 (1962).

Kadar, G. "On the product Preisach model of hysteresis". *Physica B*, Vol. 275, pp. 40-44 (2000)

Kim, S., Gopalan, V. and Gruverman, A. "Coercive fields in ferroelectrics: A case study in lithium niobate and lithium tantalate". *Applied Physics Letters*, Vol. 80, pp. 2740-2742 (2002)

Krasnoselskii, M.A. and Pokrovskii, A.V. *Systems with Hysteresis*. Berlin: Springer-Verlag (1989)

Mansingh, A. and Eswar Prasad, S.R.J. "Dielectric behavior of ferroelectric triglycine sulphate near the transition temperature". *Journal of Applied Physics*, Vol. 48, pp. 4307-4310 (1977)

Mayergoyz, I.D. *Mathematical Models of Hysteresis*. New York: Springer-Verlag (1991)

Miller, S.L., Nasby, R.D., Schwank, J.R., Rodgers, M.S. and Dressendorfer, P.V. "Device modeling of ferroelectric capacitors". *Journal of Applied Physics*, Vol. 68, pp. 6463-6471 (1990)

Miller, S.L., Schwank, J.R., Nasby, R.D. and Rodgers, M.S. "Modeling ferroelectric capacitor switching with asymmetric nonperiodic input signals and arbitrary initial conditions". *Journal of Applied Physics*, Vol. 70, pp. 2849-2860 (1991)

Lines, M.E. and Glass, A.M. *Principles and Applications of Ferroelectrics and Related Materials*. Oxford: Clarendon Press (1977)

Oti, J., Vajda, F. and Della Torre, E. "Identification of parameters in a moving model". *Journal of Applied Physics*, Vol. 69, pp. 4826-4828 (1991)

Ploss, Bernd and Heiler, Beatrix "Dielectric nonlinearity of TGS". In Schmid, G. and Sorge, G., eds., *Proceedings of the 20th Spring Conference on Ferroelectricity*, Guentersberge, 6-10 April, 1992, pp. 103-107 (1992)

Ploss, Bernd and Ploss, Beatrix "Poling of P(VDF-TrFE) with Ferroelectrically Applied Dielectric Displacement". *Ferroelectrics*, Vol. 184, pp. 107-116 (1996)

Preisach, F. "Über die Magnetische Nachwirkung". *Zeitschrift für Physik*, Vol. 94, pp. 277-302 (1935)

Scott, J.F. and Paz de Araujo, C.A. "Ferroelectric memories". *Science*, Vol. 246, pp. 1400-1405 (1989)

Taylor, D.V. and Damjanovic, D. "Domain wall pinning contribution to the nonlinear dielectric permittivity in $Pb(Zr,Ti)O_3$ thin films". *Applied Physics Letters*, Vol. 73, pp. 2045-2047 (1998)

Triebwasser, S. "Study of the second-order ferroelectric transition in tri-glycine sulfate". *IBM Journal of Research and Development*, Vol. 2, pp. 212-217 (1958)

Turik, A.V. "Theory of polarization and hysteresis of ferroelectrics". *Soviet Physics-Solid State*, Vol. 5, pp. 885-886 (1963)

Turik, A.V. "A statistical method for the investigation of repolarization processes in ferroelectric ceramics". *Soviet Physics-Solid State*, Vol. 5, pp. 1751-1753 (1964a)

Turik, A.V. "Experimental investigation of the statistical distribution of domains in a ferroelectric ceramic". *Soviet Physics-Solid State*, Vol. 5, pp. 2141-2143 (1964b)

Wong, C.K., Wong, Y.W. and Shin, F.G. "Effect of interfacial charge on polarization switching of lead zirconate titanate particles in lead zirconate titanate/polyurethane composites". *Journal of Applied Physics*, Vol. 92, pp. 3974-3978 (2002)